Distinguishing the drivers of trends in land carbon fluxes and plant volatile emissions over the past three decades

X. Yue [1], N. Unger [1], Y. Zheng [2]

[1] School of Forestry and Environment Studies, Yale University, New Haven, Connecticut 06511, USA
[2] Department of Geology and Geophysics, Yale University, New Haven, Connecticut 06511, USA

Correspondence to: X. Yue (xuyueseas@gmail.com)

Abstract

The terrestrial biosphere has experienced dramatic changes in recent decades. Estimates of historical trends in land carbon fluxes remain uncertain because long-term observations are limited on the global scale. Here, we use the Yale Interactive terrestrial Biosphere (YIBs) model to estimate decadal trends in land carbon fluxes and emissions of biogenic volatile organic compounds (BVOCs) and to identify the key drivers for these changes during 1982-2011. Driven with hourly meteorology from WFDEI (WATCH Forcing Data methodology applied to ERA-Interim data), the model simulates an increasing trend of 297 Tg C a^{-2} in gross primary productivity (GPP) and 185 Tg C a^{-2} in the net primary productivity (NPP). CO_2 fertilization is the main driver for the flux changes in forest ecosystems, while meteorology dominates the changes in grasslands and shrublands. Warming boosts summer GPP and NPP at high latitudes, while drought dampens carbon uptake in tropical regions. North of 30°N, increasing temperatures induce a substantial extension of 0.22 day a^{-1} for the growing season; however, this phenological change alone does not promote regional carbon uptake and BVOC emissions. Nevertheless, increases of LAI at peak season accounts for ~25% of the trends in GPP and isoprene emissions at the northern lands. The net land sink shows statistically insignificant increases of only 3 Tg C a^{-2} globally because of simultaneous increases in soil respiration. Global BVOC emissions are calculated using two schemes. With the photosynthesis-dependent scheme, the model predicts increases of 0.4 Tg C a^{-2} in isoprene emissions, which are mainly attributed to warming trends because CO_2 fertilization and inhibition effects offset each other. Using the MEGAN (Model of Emissions of Gases and Aerosols from Nature) scheme, the YIBs model simulates global reductions of 1.1 Tg C a^{-2} in isoprene and 0.04 Tg C a^{-2} in monoterpene emissions in response to the CO_2 inhibition effects. Land use change shows limited impacts on global carbon fluxes and BVOC emissions, but there are regional contrasting impacts over Europe (afforestation) and China (deforestation).

1 Introduction

The terrestrial biosphere interacts with the atmosphere through photosynthesis and biogenic volatile organic compound (BVOC) emissions. Annually, terrestrial ecosystems assimilate ~120 petagrams of carbon (Pg C) from the atmosphere (Beer et al., 2010), most of which reenters atmosphere through respiration and decomposition, resulting in a net global land carbon sink of 2.6 ± 0.7 Pg C a^{-1} (Le Quere et al., 2009; Sitch et al., 2015). Global BVOC emissions are estimated to be about 1 Pg C per year (Carslaw et al., 2010). These emissions are important precursors of atmospheric oxidants and aerosols, both of which affect surface air quality and exert additional regional and global chemical climate forcings (Scott et al., 2014; Unger, 2014). Observations and simulations have shown significant changes in terrestrial carbon assimilation and BVOC emissions in the past 2-3 decades (Lathiere et al., 2006; Sarmiento et al., 2010; Sindelarova et al., 2014; Sitch et al., 2015). Understanding drivers of these trends is important for the projections of future carbon fluxes, water cycle, air quality, and climatic responses.

Trends in land carbon assimilation and BVOC emissions are related to the changes in atmospheric CO_2, meteorology, and human land use land cover change perturbations. Elevated CO_2 promotes plant photosynthesis (Ainsworth and Long, 2005) but can directly inhibit isoprene productions (Arneth et al., 2007). Warming accelerates both carbon uptake and BVOC emissions when temperature is not above the thermal optimum (25-30 °C for photosynthesis and 35-40 °C for isoprene emission) for ecosystems that are not water-stressed (Farquhar et al., 1980; Guenther et al., 1993; Piao et al., 2013). Additional warming above thermal optimum may decrease photosynthesis but still promote respiration, reducing net carbon uptake by plants (Liang et al., 2013). Increased temperatures also indirectly influence carbon exchange and BVOC emissions through the extension of growing season (Piao et al., 2007). Drought decreases gross primary productivity (GPP) and net primary productivity (NPP) (Zhao and Running, 2010), but may temporally enhance isoprene emissions (Monson et al., 2007). Land use change affects the regional carbon budget and BVOC emissions through either additional

emissions or land cover changes due to deforestation, forest management, and agricultural activities (Lathiere et al., 2006; Houghton, 2010).

Estimates of recent decadal global trends in the land carbon budget and BVOC emissions are limited and uncertain due to the lack of observations. The earliest site-level measurements of land carbon fluxes were set up in the 1990s (Wofsy et al., 1993). The flux tower data sets provide long-term records of regional carbon exchange with high precision but low spatial representation. In contrast, satellite products, such as GPP and NPP retrievals from the Moderate Resolution Imaging Spectroradiometer (MODIS) (Zhao et al., 2005) and isoprene emissions based on tropospheric formaldehyde columns from the Global Ozone Monitoring Experiment (Palmer et al., 2006), improve the spatial coverage but usually are available for only a relatively short time period (months to several years) and suffer from systematic biases when compared with ground measurements (e.g., Heinsch et al., 2006; Marais et al., 2012). Terrestrial biosphere models, evaluated with both site-level and satellite-based observations, are useful tools to estimate trends and attribute drivers of changes in land carbon fluxes and BVOC emissions (e.g., Mao et al., 2013; Stavrakou et al., 2014; Sitch et al., 2015).

In this study, we use the Yale Interactive Terrestrial Biosphere Model (YIBs, Yue and Unger, 2015) driven with long-term reanalysis meteorology to study the global trends of land carbon fluxes and BVOC emissions over the past three decades. The YIBs model is a process-based vegetation model including complete land carbon cycle (photosynthesis, plant/soil respiration, carbon allocation, and tree growth), plant phenology (Yue et al., 2015), and two independent schemes of BVOC emissions (Zheng et al., 2015). Simulated carbon fluxes has been fully validated with carbon fluxes from 145 flux tower sites and multiple satellite products (Yue and Unger, 2015). The major goals of this study are to identify: (1) the dominant drivers of the 30-year trends in carbon fluxes and BVOC emissions from elevated CO_2, changes in meteorology (temperature, radiation, and soil moisture), and human land use change; (2) the feedback of biosphere, including changes in phenology and leaf area index (LAI), to the trends of land carbon uptakes and BVOC

105 emissions; and (3) the discrepancies in BVOC trends due to application of different
106 isoprene emission schemes.
107
108
109 **2 Data and methods**
110
111 **2.1 Observations and benchmark products**
112
113 We use long-term global measurements of LAI, GPP, and NPP to validate the simulated
114 trends. The LAI dataset for 1982-2011 is retrieved based on the Normalized Difference
115 Vegetation Index (NDVI) from Global Inventory Modeling and Mapping Studies
116 (GIMMS) with 1/12 degree resolution and a 15-day interval (Zhu et al., 2013). We also
117 use LAI data for 2000-2011 from the MODIS (http://modis.gsfc.nasa.gov/). GPP
118 benchmark products of 1982-2011 are upscaled from the FLUXNET eddy covariance
119 measurements using an ensemble of regression trees (Jung et al., 2009). As a comparison,
120 we also use the GPP and NPP datasets for 2000-2011 from the MODIS, which have been
121 developed based on remote sensing of biome parameters and assimilated meteorology
122 (Zhao et al., 2005). All the datasets are interpolated to the monthly interval at the 1°×1°
123 off-line YIBs model resolution.
124
125 **2.2 Model**
126
127 The YIBs model is a process-based terrestrial vegetation model that simulates the land
128 carbon budget and dynamic tree growth (Yue and Unger, 2015). The model adapts
129 routines from the mature TRIFFID (Cox, 2001) and CASA (Schaefer et al., 2008) models
130 with special updates in the parameterizations of ozone vegetation damage (Yue and
131 Unger, 2014), plant phenology (Yue et al., 2015), and the photosynthesis-dependent
132 isoprene emission (Unger et al., 2013). The model simulates carbon uptake for 9 plant
133 functional types (PFTs) including tundra, C3/C4 grass, shrubland, deciduous broadleaf
134 forest (DBF), ENF evergreen needleleaf forest (ENF), evergreen broadleaf forest (EBF),
135 and C3/C4 cropland. The vegetation biophysics calculates leaf-level photosynthesis using

the well-established Farquhar scheme (Farquhar et al., 1980; von Caemmerer and Farquhar, 1981) and the stomatal conductance model of Ball and Berry (Collatz et al., 1991). The canopy radiative transfer scheme computes direct and diffuse photosynthetically active radiation (PAR) for sunlit and shaded regions for an adaptive number of layers. The leaf photosynthesis is then integrated over all canopy layers to generate the GPP.

Part of the assimilated carbon is used for maintenance and growth respiration, and the rest is allocated among different pools for plant development. The model calculates phenology for deciduous forests using cumulative temperature summation with additional constraints from chilling and photoperiod (Yue et al., 2015). The phenology of shrubland and grassland is jointly determined by the temperature- and drought-dependent metrics. The LAI is then updated daily based on phenology and the net carbon assimilation. The soil respiration scheme considers carbon flows among 12 biogeochemical pools, including 3 live pools and 9 dead pools. The land carbon source or sink is calculated as the difference between the net carbon assimilation and soil respiration.

The YIBs model incorporates two independent leaf-level isoprene emission schemes embedded within the exact same host model framework (Zheng et al., 2015). The photosynthesis-based (PS_BVOC) isoprene scheme calculates emissions based on the electron transport-limited photosynthesis rate, canopy temperature, and intercellular CO_2 concentrations (Arneth et al., 2007; Unger et al., 2013). The Model of Emissions of Gases and Aerosols from Nature (MEGAN) scheme applies commonly used leaf-level empirical functions of light and canopy temperature. Both schemes implement CO_2 inhibition effects on BVOC emissions parameterized as a reciprocal empirical function of intercellular [CO_2] following the observations from Possell et al. (2005). For monoterpene emissions, the YIBs model applies the same temperature-dependent scheme as Lathiere et al. (2006) but with CO_2-inhibition effects. The leaf-level BVOC emissions are integrated over the multiple canopy layers following the same approach as GPP to obtain the total canopy-level emissions.

YIBs can be used in three different configurations with increasing complexity: (1) off-line local site level, which is driven with hourly measurements of CO_2 concentrations and meteorology at flux tower sites; (2) off-line global forced with spatially uniform but annually updated CO_2 concentrations and hourly gridded reanalysis meteorology; (3) on-line coupled to the NASA ModelE2 driven with simulated meteorology by the GCM every half hour. At the site level, YIBs simulates reasonable seasonality (correlation coefficient R>0.8) of GPP at 121 out of 145 flux-tower sites with biases in magnitude ranging from -19 to 7 % depending on PFTs. On the global scale, the offline model simulates an annual GPP of 125 ± 3 Pg C and net ecosystem exchange (NEE) of -2.5 ± 0.7 Pg C for 1982-2011, with seasonality and spatial distribution consistent with both satellite observations and benchmark synthesis products (Yue and Unger, 2015). However, the model does not include a fully coupled carbon-nitrogen cycle, which may overestimate CO_2 fertilization effects. In addition, phenology of evergreen trees is set to constant value of 1, leading to underestimation of phenological feedbacks to flux trends. In this study, we use the (2) off-line global version of the model, which is driven with global meteorology reanalysis data and observed CO_2 concentrations.

2.3 Simulations

We apply observed historical atmospheric CO_2 concentrations from the fifth assessment report (AR5) of the Intergovernmental Panel on Climate Change (IPCC) (Meinshausen et al., 2011). We apply an annually-varying historical transient land cover dataset (Oleson et al., 2013), which is developed based on a combination of remote sensing data from both MODIS (Hansen et al., 2003) and the Advanced Very High Resolution Radiometer (AVHRR) (Defries et al., 2000), and with land use change from Hurtt et al. (2011). We use hourly meteorological variables for 1980-2011 from the WATCH Forcing Data methodology applied to ERA-Interim data (WFDEI, Weedon et al., 2014). The WFDEI reanalysis is an update of the WATCH Forcing Data (WFD), which is developed based on the European Centre for Medium-range Weather Forecasts (ECMWF) ERA-40 reanalysis (Uppala et al., 2005). Meteorological variables applied include surface air temperature, specific humidity, wind speed, surface pressure, total PAR, and soil

temperature and wetness. All of the forcing data are interpolated to the 1°×1° model resolution at the hourly interval.

We perform 10 sensitivity simulations to distinguish driving factors for the changes in land carbon fluxes and BVOC emissions in the past 3 decades (Table 1). The control simulation (CO2_MET_LUC) uses interannually-varying meteorology, [CO_2], and land cover for 1980-2011. The CO2_MET run is the same as the control simulation but prescribes land cover at the year 1980. Three single-factor runs prescribe most boundary conditions at the year 1980 but allow the interannual variations of [CO_2] (CO2_ONLY), land cover (LUC_ONLY), and meteorology (MET_ONLY) respectively. Results from these runs are compared with that of control simulation to determine the dominant drivers of simulated trends. To understand the impact of individual meteorological variables, three additional runs are performed with fixed (or recycled) [CO_2], land cover, and all meteorology at year 1980 but one field varying for 1980-2011 each time, including temperature (TEMP_ONLY), PAR (PAR_ONLY), and soil wetness (SOILW_ONLY). Finally, two runs are performed to examine feedback of biospheric changes. LAI_ONLY prescribes all boundary conditions at the starting year 1980 but implements the year-to-year LAI simulated by the control run. PHEN_ONLY also prescribes all forcings at the starting year except for the year-to-year phenology from control simulation. All simulations are initialized following the same spin up process (Yue and Unger, 2015) and are integrated for 1980-2011.

3 Results

3.1 Drivers of trends in LAI

Observations show an increasing trend of LAI on most of vegetated continents, especially in Europe, northern and eastern Asia, central Africa, and southeastern U.S. in the past 3 decades (Fig. 1a). The simulation with year-to-year [CO_2], land cover, and meteorology reproduces the magnitude of trend in Europe and the sign of trend in northern Asia,

229 eastern U.S., central Asia, and Australia (Fig. 1b). The model predicts negative changes
230 in central Africa, western U.S., eastern Asia, and the east of South America, which are
231 inconsistent with satellite observations. These negative trends are mainly contributed by
232 the changes in meteorology (Fig. 1e), except for that in East Asia where land cover
233 changes due to human activities result in the decline of LAI (Fig. 1f). Without the land
234 use perturbation, the negative LAI trend in East Asia is weakened and the prediction is
235 closer to observations (Fig. 1c). For the individual drivers, CO_2 fertilization leads to
236 widespread increases in LAI (Fig. 1d), meteorology causes dipole changes on most
237 continents (Fig. 1e), and land use change generally results in negative trends (Fig. 1f).
238 Regionally, simulation CO2_MET_LUC shows a positive trend of 0.0035 m^2 m^{-2} a^{-1} in
239 Europe (Table 2), close to the observed value of 0.0049 m^2 m^{-2} a^{-1} (Fig. 1a). In other
240 areas, simulated LAI trends are either underestimated (by 87% in Amazon, 78% in North
241 America, and 48% in Central Africa) or opposite in sign (East Asia and Indonesia)
242 compared to observations. Such inconsistencies indicate the limit of model simulations,
243 but may also in part result from the uncertainties in the satellite measurements (see
244 section 4.1).
245
246 **3.2 Drivers of trends in land carbon fluxes**
247
248 Predicted GPP and NPP trends show similar spatial pattern as that of LAI (Figs. 2a and
249 2c). However, regional trends are all positive in the main continents and on the global
250 scale (Tables 2 and 3). Tropical areas are experiencing maximum changes, especially in
251 Central Africa (GPP by 83.3 Tg C a^{-2} and NPP by 51.7 Tg C a^{-2}) and the Amazon (52.7
252 and 27.1 Tg C a^{-2}). In the Northern Hemisphere (NH), changes are significant in Europe
253 (53.4 and 33.2 Tg C a^{-2}), East Asia (42.4 and 27.2 Tg C a^{-2}), and North America (13.6
254 and 9.7 Tg C a^{-2}). 30-year historical observations of GPP and NPP are not available.
255 Therefore, we compare YIBs predictions with MODIS land carbon fluxes over the more
256 recent period of 2000-2011 (Fig. 3). Different from the 30-year trend, land carbon fluxes
257 over the recent decade show negative trends in southeastern U.S., southern Africa,
258 eastern Australia, and central and northern Asia (Figs. 3a and 3c). Most of these changes

are consistent with the MODIS observations (except for the U.S., Figs. 3b and 3d) and are attributed to the drought tendency in the past decade (Zhao and Running, 2010).

For the 30-year trend, both CO_2 and meteorology are playing important roles (Figs. 2b and 2d). CO_2 fertilization dominates the GPP and NPP trends of tropical forests in the Amazon, central Africa, and Indonesia, and ENF and DBF in boreal North America, eastern Europe, and central and northern Asia. Land use change plays a limited role in land carbon cycle flux trends over the past 3 decades, except for some areas in northern Africa. Meteorological forcing drives changes in land carbon fluxes for tundra in subarctic regions, C3 grasslands in the central U.S. and southern Africa, C4 grasslands in central Africa and the east of South America, and shrublands in Australia and southern Asia. Soil wetness plays the dominant role in the tropical and subtropical areas (Fig. 4b). The drought tendency in the western U.S., central Africa, and the east of South America (Fig. S1d) results in the regional decline of land carbon fluxes (Fig. 4a). In contrast, the increasing wetness in the northern Amazon and southern Africa leads to the enhancement of regional GPP. Warming is the main cause for the GPP trends over the subarctic areas (Fig. 4b). Contribution of PAR is limited, except for some areas in the eastern Europe.

The simulated net ecosystem productivity (NEP) shows weaker trends compared with GPP and NPP (Fig. 2e), because NEP is offset by the significant trends in heterotrophic respiration (Rh) (Table 2). Regionally, the YIBs model predicts enhanced net land carbon uptake in boreal North America, northern Asia, and southern Africa but reduced NEP in the central U.S., the Amazon, central Africa, eastern Europe, and East Asia. The simulated global NEP trends (Fig. 5d) are in broad agreement with the comprehensive bottom-up estimates by Pan et al. (2011), who found slightly decreasing net carbon uptake by global established forests (without human perturbations in the tropics but with afforestation in subtropical areas) in 2000-2007 relative to that in 1990-1999. Attribution analysis shows that the NEP trends are mainly driven by the changes in meteorological forcings (Fig. 2f), because CO_2 fertilization enhances both NPP and Rh with similar magnitude (Fig. 5).

On the global scale, GPP, NPP, and Rh increase respectively by 298, 185, and 181 Tg C a^{-2} in the past 3 decades (Table 3). The long-term trends of carbon fluxes are mainly driven by CO_2 fertilization, while the interannual variability is related to meteorological forcings (Fig. 5). Warming alone decreases GPP especially in tropical forests (not shown) but increases autotrophic respiration (Ra), leading to global reductions of 56 Tg C a^{-2} in NPP and 10 Tg C a^{-2} in NEP (Table 3). Drought alone strongly decreases GPP, especially for tropical grassland and shrubland (Fig. 4), leading to reductions of 51 Tg C a^{-2} in NPP and 13 Tg C a^{-2} in NEP. Trends in PAR do not affect GPP and NPP, but may decrease NEP by 23 Tg C a^{-2} because soil respiration is slowly increasing to reach the equilibrium. Land use change has very limited impacts on the trends of carbon fluxes, though it induces relatively large reductions in NEP (Table 3).

3.3 Drivers of trends in BVOC emissions

Simulated isoprene emission trends are sensitive to the choice of modeling scheme. With the PS_BVOC scheme, global isoprene emissions increase by 0.4 Tg C a^{-2} during 1982-2011. Large enhancements are predicted in central Africa (0.25 Tg C a^{-2}) and Europe (0.16 Tg C a^{-2}), while moderate reductions are found in the western U.S., eastern South America, and East Asia (Fig. 6a). Drought accounts for the decline of isoprene emissions in the U.S. and South America, but land use change is the main driver for the reductions in East Asia (Fig. 6b). Increasing [CO_2] promotes photosynthesis but meanwhile inhibits BVOC emissions, leading to offsetting CO_2 effects on isoprene. Consequently, the global isoprene emission is mainly driven by meteorological changes (Fig. 6b). In contrast, using MEGAN scheme, the YIBs model simulates a global reduction of 1.1 Tg C a^{-2} for isoprene emissions (Fig. 6c). Strong declines are found in the tropical rainforest, for example in the Amazon (-0.43 Tg C a^{-2}), central Africa (-0.14 Tg C a^{-2}), and Indonesia (-0.16 Tg C a^{-2}) (Fig. 6c). The MEGAN scheme is sensitive to both light and temperature (Guenther et al., 1995). The strong positive brightening trends in PAR in Europe (Fig. S1b) promote isoprene emissions there. The positive impacts of NH warming (Fig. S1a) are compensated by CO_2 inhibition, leading to small changes in isoprene emissions (Fig. 6c). In the tropical areas, where trends of temperature and PAR are limited, CO_2

inhibition results in strong reductions of BVOC emissions. Monoterpene emissions show a global reduction of 0.04 Tg C a^{-2} over the past 3 decades (Fig. 6e).

3.4 Feedback of biospheric changes to the trends

Due to the changing climate and CO_2 fertilization, the biosphere is experiencing significant changes in the past 3 decades. The most evident alterations include LAI changes in peak season and phenological changes in growing and falling seasons. In this section, we explore the feedback of these biospheric changes to the carbon uptake and BVOC emissions.

3.4.1 Impacts of LAI changes

Sensitivity run LAI_ONLY retains the trends in LAI but prescribes other forcings. In this simulation, trends in GPP (Fig. S2a) and NPP (Fig. S2c) generally follow that in LAI (Fig. 1b), but with smaller magnitude relative to those in control simulations (Figs. 2a and 2c). LAI in the north of 30°N shows widespread increases in both observations and simulations (Figs. 1a and 1b). Over these northern lands, the unit change in leaf area leads to enhancement of regional GPP by 32 Pg C a^{-1}, much lower than the response of 116 Pg C a^{-1} LAI^{-1} for the simulation including CO_2 fertilization and climate forcings (Fig. 7a). In the tropical areas, both positive and negative LAI trends are predicted due to the competition between CO_2 fertilization and drought effects (Fig. 1). As a result, LAI-induced GPP and NPP changes show patchy distributions at tropics (Fig. S2a and S2c), leading to moderate changes in the global carbon assimilations (Table 3).

Trends in isoprene emission (calculated with the PS_BVOC scheme) also follow that of LAI, except that leaf expansion results in decreased emissions at high latitudes (~60°N, Fig. S2e). The cause for such inconsistency is unclear, but might be because the denser leaves reduce radiation penetrating to lower canopy layers. Such impact would only affect BVOC emissions at high latitudes because PAR is usually limiting near subarctic areas. In most of the subtropical areas, increased LAI leads to enhanced isoprene

352 emissions. On average, unit change in LAI at north of 30°N leads to enhanced isoprene
353 emissions by 43 Tg C a^{-2}, only 25% of the magnitude in simulation CO2_MET (Fig. 7b).
354 A similar ratio of 23% is achieved for MEGAN isoprene emissions. These results are
355 consistent with that for GPP (Fig. 7a), suggesting that CO_2 fertilization and
356 meteorological changes are the main drivers for the changes in carbon uptake and BVOC
357 emissions, even over the northern lands where the most evident changes in LAI are
358 observed.
359
360 **3.4.2 Impacts of phenological changes**
361
362 Plant phenology, which is the timing of budburst and leaf fall, is closely related to
363 temperature, moisture, and photoperiod and thus is experiencing significant changes in
364 the past decades following climate change (Jeong et al., 2011; Keenan et al., 2014;
365 Buitenwerf et al., 2015; Yue et al., 2015). Extension of the growing season has the
366 potential to promote carbon uptake of forests (e.g., Piao et al., 2007; Richardson et al.,
367 2009). Yet such inference requires careful interpretation because the phenological
368 changes are usually accompanied with warming and elevated [CO_2], both of which are
369 also contributing to the enhancement of carbon fluxes. Phenological changes are also
370 expected to affect BVOC emissions, however, such investigations are still missing
371 (Richardson et al., 2013). With the YIBs model, we evaluate the impacts of the growing
372 season extension on both carbon uptake and BVOC emissions by isolating long-term
373 phenological trends from changes in temperature and [CO_2].
374
375 The YIBs model simulates advanced spring and delayed autumn over most areas in NH
376 (Fig. S3). Budburst dates advance on average by 0.16 days a^{-1} in Europe and 0.15 days a^{-1}
377 in East Asia (Table 2), but with moderate changes or even delays in northwestern Asia
378 and eastern Siberia (Fig. S3a). Spring is earlier by 0.14 days a^{-1} in eastern U.S. while
379 delayed by 0.15 days a^{-1} in northwestern U.S. and southeastern Canada, leading to a
380 minor advance of 0.01 days a^{-1} over North America. Dormancy onset dates are largely
381 delayed in eastern Europe and northwestern Asia (~0.3 day a^{-1}), western U.S. (~0.1 day a^{-1}),
382 boreal Canada (~0.1 day a^{-1}), and northeastern China (~0.1 day a^{-1}) (Fig. S3b).

383 Advanced autumn (~0.1 day a^{-1}) is predicted in northern Asia. Most of these changes are
384 consistent with observations from remote sensing data (Jeong et al., 2011), except for
385 some discrepancies in the magnitude. The predicted phenological trends mainly follow
386 the long-term changes of surface air temperature, especially that in April (for spring) and
387 September (for autumn) (Fig. S4). Sensitivity tests without chilling requirement and
388 photoperiod limit show similar changes (Yue et al., 2015), suggesting that temperature
389 changes dominantly drive the trends of forest phenology in the past 3 decades.
390
391 On average, the YIBs model simulates advanced budburst by 0.12 day a^{-1} and delayed
392 dormancy onset by 0.09 day a^{-1} at north of 30°N in the past 3 decades (Figs. 8a and 8b).
393 Observations based on remote sensing greenness show trends of -0.11 day a^{-1} for onset
394 and 0.25 day a^{-1} for offset during 1990-2009 (Zhu et al., 2013). An ensemble prediction
395 based on 9 terrestrial models yields an advance of 0.08 ± 0.13 day a^{-1} for onset and a
396 delay of 0.22 ± 0.1 day a^{-1} for offset (Sitch et al., 2015). Our predictions are in broad
397 agreement with these estimates though the autumn delay is less, likely because the
398 positive trend of offset is weaker for the recent decade (Jeong et al., 2011).
399
400 We plot the annual total GPP and isoprene emissions at north of 30°N against the length
401 of growing season for 1982-2011 (Figs. 8c and 8d). In the CO2_MET run, the 1-day
402 extension is correspondent to increases of 0.17 Pg C a^{-1} in GPP and 0.34 Tg C a^{-1} in
403 isoprene emissions. If only temperature is allowed to vary, the phenological trend
404 remains the same while the increases of GPP and isoprene emissions are largely
405 weakened. In the TEMP_ONLY run, the 1-day extension in growing season is
406 accompanied by increases of 0.05 Pg C a^{-1} in GPP and 0.25 Tg C a^{-1} in isoprene
407 emissions. The changes in BVOC emissions are not as dramatic as those of GPP because
408 CO_2 has both enhancing and suppressing impacts on the former. If we further exclude
409 temperature effects (PHEN_ONLY run), GPP increases only by 0.01 Pg C a^{-1} while
410 isoprene emissions decrease by 0.1 Tg C a^{-1}, both of which are not statistically
411 significant, suggesting that the phenological change alone does not promote either GPP
412 or isoprene emissions. There are two reasons for this apparent contradiction. First, the
413 extension of the growing season occurs in shoulder months, usually in May and

September, when both GPP and BVOC emissions and their changes are much smaller compared to that in peak months (Fig. S5). Second, phenological changes are not uniform in space. As Fig. S3 shows, both positive and negative changes are predicted for budburst and dormancy onset dates. Such spatial inhomogeneity, in combination with the discrepancies in regional vegetation types and meteorological conditions, result in varied responses in GPP (Fig. S2b) and isoprene emissions (Fig. S2f).

Plant phenology at lower latitudes (30°S-30°N) is also experiencing dramatic changes, though such changes are diverse in phase, magnitude, or both (Buitenwerf et al., 2015). In the model, tropical phenology is mainly driven by soil wetness and as a result exhibits large changes in the past 3 decades (not shown). These changes lead to a reduction of 42 Tg C a^{-1} in GPP at the tropics (Fig. S2b), which accounts for 14% of global GPP trend but with the opposite sign (Table 3), suggesting additional inhibition of drought on carbon cycle. A similar conclusion applies for BVOC emissions (Fig. S2f), though experiments suggest that isoprene production has some tolerance to mild drought conditions (e.g., Pegoraro et al., 2006). However, changes in drought-dependent phenology are very uncertain and observations are not available for evaluation. We assume that phenological changes may have larger impacts on both carbon assimilation and BVOC emissions at tropical areas than that at higher latitudes.

4 Discussion

4.1 Uncertainties in observations

Terrestrial biosphere modeling is a useful tool to identify drivers of long-term changes in land carbon fluxes. The reliability of simulations is dependent on the availability of observations for model validation. In this study, we use 30-year LAI observations from the LAI3g product (Zhu et al., 2013) and 12-year GPP from MODIS (Zhao et al., 2005), both of which are remote sensing retrievals, to validate the simulated trends (Figs. 1 and 3). We found the offline global model biases against both fields, especially for LAI (Fig.

1). Such discrepancies may in part result from the uncertainties in measurements themselves. As a check, we compare the derived LAI trends from LAI3g with retrievals from MODIS for the overlap period of 2000-2011 (Figs. S6a and S6b). Global LAI significantly increases in LAI3g but show widespread reductions in MODIS, especially over subtropical areas. Simulated trends (CO2_LUC_MET) are closer to the estimates with MODIS, especially for the changes in the NH (not shown). Meanwhile, we compare the derived GPP trends from MODIS with that upscaled from FLUXNET data using an ensemble of regression trees (Jung et al., 2009) for 2000-2011 (Figs. S6c and S6d). The two products show similar trends over most areas except for some discrepancies in tropical areas and the eastern U.S. Simulated GPP trends match results from Jung et al. (2009) better than that from MODIS (Fig. 3a). However, we do not use Jung et al. (2009) to validate simulations for 1982-2011 because the earliest flux tower observations began only in middle 1990s. The large discrepancies in the observed trends among different data sets not only indicate the importance of model evaluations with multiple products, but also put forward the necessity of data inter-comparisons and algorithm improvements to alleviate uncertainties in observations.

4.2 Comparisons with other modeling studies

The YIBs model predicts NPP trends of 67.4 Tg C a^{-2} in northern land (25-90°N) and 98.1 Tg C a^{-2} in tropical land (15°S-25°N), similar to the ensemble estimates of 63 ± 22 and 102 ± 34 Tg C a^{-2} for 1990-2009 based on 9 terrestrial biosphere models (Sitch et al., 2015). However, the simulated NPP trend is only 19.8 Tg C a^{-2} in southern land (15-90°S), much lower than the ensemble mean value of 53 ± 31 Tg C a^{-2} in Sitch et al. (2015). As for the NEP, the YIBs predicts trends of 2.0 Tg C a^{-2} in northern land, 1.0 Tg C a^{-2} in tropical land, and -0.3 Tg C a^{-2} in southern land, much smaller in magnitude compared with the -2.0 ± 12, 36.0 ± 13, and 21 ± 17 Tg C a^{-2} estimated by Sitch et al. (2015). However, their predictions are insignificant ($p > 0.05$) for 9, 5, and 7 out of 9 models in the northern, tropical, and southern land respectively, suggesting that the strengthening uptake by terrestrial ecosystem is not robust.

Stavrakou et al. (2014) investigated isoprene emissions over Asia during 1979-2012 using the MEGAN scheme and taking into account both climate and land-use changes. Their results showed widespread increases in the emissions over China but moderate decreases in Indonesia. In contrast, the YIBs model with the MEGAN scheme simulates widespread reductions in the same areas for 1980-2011 (Fig. 6c). The discrepancies between studies are accounted for by differences in the drivers including land cover change, meteorology, and CO_2 inhibition effects. The YIBs model is driven with land cover data from Hurtt et al. (2011), which estimates an increase of crop (non-isoprene emitter) fraction in East China by 0.32% per year in the last 3 decades, at the cost of the coverage loss by 0.12% a^{-1} for DBF and 0.14% a^{-1} for ENF (strong BVOC emitters). However, the data from Ramankutty and Foley (1999), used by Stavrakou et al. (2014) with updates to 2007, show a reduction of the crop fraction over East China for the similar period. In addition, the ERA-Interim PAR used in Stavrakou et al. (2014) shows an increasing trend in southeast China (c.f. their Fig. 5c). On the contrary, the WFDEI PAR for YIBs exhibits a declining trend in the same region (Fig. S1b), leading to a reduction in isoprene emissions. The WFDEI surface solar radiation is based on the ERA-Interim radiation but is adjusted using the average cloud cover from the Climatic Research Unit (CRU) and taking into account the effects of interannual changes in atmospheric aerosols (Weedon et al., 2011). Finally, the YIBs simulations include CO_2 inhibition effects on BVOC emissions, which were neglected in Stavrakou et al. (2014).

Naik et al. (2004) predicted a global trend of 1.3 Tg C a^{-2} for isoprene emissions during 1971-1990 using the Integrated Biospheric Simulator (IBIS) driven with monthly mean CRU meteorology. Lathiere et al. (2006) estimated an increasing global trend of 0.3 Tg C a^{-2} for 1983-1995 using the ORCHIDEE (Organizing Carbon and Hydrology in Dynamic EcosystEms) vegetation model driven with sub-daily variables from the NCEP/DOE (National Center for Environmental Predictions/Department of Energy) Reanalysis 2. Muller et al. (2008) reported a global increase of 4.5 Tg C a^{-2} for 1995-2006 using a canopy environmental model and the NCEP meteorological data. In contrast to these previous studies, YIBs with the MEGAN scheme simulates a decreasing trend of ~1 Tg C a^{-2} in the past 3 decades. The main cause of the discrepancy in the sign of change is the

missing CO_2 inhibition effects in the previous studies. In addition, differences in vegetation models, meteorological forcings, and time frames of investigation also likely contribute. The YIBs result is consistent with a recent study by Sindelarova et al. (2014), who reported a decreasing trend of ~1.2 Tg C a^{-2} for global isoprene emissions during 1980-2010 using the MEGAN scheme and inclusion of a CO_2 inhibition parameterization from Heald et al. (2009).

4.3 Impacts of CO_2 effects

Similar to the multi-model ensemble predictions (Sitch et al., 2015), we found that global trends in carbon fluxes are dominantly driven by CO_2 fertilization (Figs. 2 and 5). In the YIBs, the global responses to elevated [CO_2] is 0.2% ppm^{-1} for GPP and 0.27% ppm^{-1} for NPP, with relatively uniform spatial distribution (Figs. S7a and S7b). The GPP response falls within the range of 0.05-0.21% ppm^{-1} predicted by 10 terrestrial models (Piao et al., 2013) and that of 0.01-0.32% ppm^{-1} observed from multiple free-air CO2 enrichment (FACE) sites (Ainsworth and Long, 2005). The NPP response is higher than the model ensemble of 0.16% ppm^{-1} (Piao et al., 2013) and the observed median value of 0.13% ppm^{-1} (Norby et al., 2005), suggesting that CO_2 fertilization to NPP may be overestimated in the YIBs. One possible cause is the omission of N limitation in the model, which could reduce CO_2 responses by half (Piao et al., 2013). Elevated [CO_2] leads to increases of 0.023 Pg C a^{-1} ppm^{-1} in NEP, within the multi-model range of 0.003-0.06 Pg C a^{-1} ppm^{-1} (Piao et al., 2013).

Responses of BVOC emissions to elevated [CO_2] are different between PS_BVOC and MEGAN schemes (Figs. S7c and S7d). PS_BVOC includes both CO_2 fertilization (on photosynthesis) and inhibition (on isoprene) effects, leading to moderate but generally positive changes in isoprene emissions. In contrast, emissions from the MEGAN scheme are not dependent on foliar photosynthesis and as a result only CO_2 inhibition is enforced. Chamber experiments show contrary tendencies for photosynthesis and isoprene in response to elevated [CO_2] (Possell et al., 2005), supporting the simulations with MEGAN. In addition, the magnitude of CO_2 inhibition implemented in MEGAN (-0.25%

538 ppm^{-1}) is close to observations (-0.26% ppm^{-1}) in Possell et al. (2005). However, most of
539 these experiments are conducted for short-term period and cannot detect LAI changes due
540 to the long-term CO_2 fertilization. In addition, the impacts of CO_2 are dependent on
541 species and environmental conditions (ambient temperature and light availability). For
542 example, Buckley (2001) found almost no responses in isoprene emissions to the elevated
543 [CO_2] for oak trees. Furthermore, experiments with high temperature and/or light density
544 show increasing isoprene at elevated [CO_2] (Sun et al., 2013). These studies suggest that
545 the real responses of isoprene emissions to CO_2 under long-term climate change may not
546 be so linear as predicted in MEGAN scheme. More sensitivity experiments and long-term
547 samplings are required to identify CO_2-isoprene relationships on broad range of biomes
548 and locations.
549
550 **4.4 Impacts of meteorology**
551
552 Predicted long-term trends show large deviations against observations at tropical areas
553 (Fig. 3), where meteorology plays important and complex roles. Responses of carbon
554 fluxes to temperature are more diverse than to CO_2 (Figs. S8a and S8b). In the YIBs,
555 negative responses of GPP and NPP are predicted in tropical areas, where soil moisture
556 availability limits plant functions (e.g. stomatal conductance) to the increased
557 temperature. Furthermore, for tropical rainforests where ambient temperature is higher
558 than optimal photosynthetic temperature (25-30°C), additional warming decreases carbon
559 assimilation, especially for NPP because of simultaneous increases in plant respiration
560 (Liang et al., 2013). On the contrary, warming leads to enhanced GPP and NPP at wetter
561 and cooler areas in the NH subtropics. Such spatial pattern is consistent with multi-model
562 ensemble predictions (Piao et al., 2013). On the global scale, warming results in changes
563 of -0.7% $°C^{-1}$ for GPP in YIBs, falling within the range of -1.6-1.4% $°C^{-1}$ estimated by 10
564 models (Piao et al., 2013). Predicted NPP responses of -15-6% $°C^{-1}$ (Fig. S8b) is not so
565 positive as the measurements of -8-40% $°C^{-1}$, probably because most of current warming
566 experiments are located in subtropics of NH (Wu et al., 2011). Elevated temperature
567 changes NEP by -1.4 Pg C a^{-1} $°C^{-1}$, also within the multi-model range of -5~-1 Pg C a^{-1}
568 $°C^{-1}$ (Piao et al., 2013). Simulated isoprene emissions with PS_BVOC show similar

569 warming responses as that of carbon fluxes (Fig. S8c), except for tropical rainforests
570 where the former is positive while the latter is negative. Such decoupling is attributed to
571 the differences in optimal temperatures between isoprene (35-40 °C) and photosynthesis
572 (25-30 °C). Simulations with MEGAN scheme show very strong temperature dependence
573 of 6-15% $°C^{-1}$ (Fig. S8d), consistent with measurements of 5-20% $°C^{-1}$ for aspen
574 (Niinemets and Sun, 2015) and 9-12% $°C^{-1}$ for oak (Li et al., 2011). However,
575 experiments with some other species (e.g. spruce in Kivimaenpaa et al. (2013)) show no
576 responses or moderate ones, suggesting that warming sensitivity of isoprene emissions
577 might be dependent on species and ambient conditions.
578
579 Responses to PAR are mostly positive and distributed evenly, with global sensitivity of
580 0.3% W^{-1} m^2 for GPP and 0.5% W^{-1} m^2 for NPP (Figs. S9a and S9b). Isoprene emissions
581 from both PS_BVOC and MEGAN schemes show similar responses to PAR, with larger
582 sensitivity in subtropics than that in tropics (Figs. S9c and S9d), likely because the
583 ambient PAR is higher at lower latitude, leading to slower responses of isoprene
584 emissions to the unit changes of light (Guenther et al., 1993). YIBs simulations show that
585 PAR is not the driver of long-term trends in carbon fluxes and BVOC emissions (Fig. 4),
586 likely because changes in solar radiation is limited in the past 3 decades (Figs. S1b).
587
588 Soil moisture dominates climate-driven flux changes in tropical areas (Fig. 4). In YIBs
589 model, changes in soil water availability affect carbon assimilation through the alteration
590 of leaf stomatal conductance and plant phenology (especially for shrublands and
591 grasslands in arid regions). Both GPP and NPP show strong responses to soil wetness
592 variations, especially over tropics where >10% changes are found for every increase of
593 0.01 in soil wetness at 1.5 m (Figs. S10a and S10b). On the global scale, GPP changes by
594 4.7% 0.01^{-1} and NPP by 5.5% 0.01^{-1} in response to soil wetness. Although experiments
595 also show rapid reductions in carbon assimilation due to drought stress (e.g., Ruehr et al.,
596 2012; Xia et al., 2014), the magnitude of such influence is difficult to evaluate because
597 different metrics and depths of soil water are used in measurements. Isoprene emissions
598 from PS_BVOC show similar soil-wetness responses to that of GPP (Fig. S10c),
599 indicating that drought reduces BVOC emissions. However, observations show

insignificant changes of isoprene with mild drought stress (e.g., Pegoraro et al., 2006), though such drought tolerance is strongly weakened at severe drought and/or warm conditions (Centritto et al., 2011). Consistent with these experiments, MEGAN scheme does not include drought inhibition on isoprene emissions. Simulations with YIBs show large responses of BVOC to soil wetness in tropical areas (Fig. S10d), mainly because of the changes in drought-dependent phenology.

4.5 Impacts of land use change

Changes of land use show moderate impacts on global carbon budget (Fig. 2) and BVOC emissions (Fig. 6) in the past 3 decades, though regional perturbations are found in China and Europe. The afforestation in Europe helps promote regional carbon uptake, resulting in more reasonable trends in LAI compared with remote sensing data (Fig. 1). However, the expansion of crop in China leads to a reduction in LAI, which is not supported by the satellite data. One possible cause is the uncertainty in crop fraction, because data from Hurtt et al. (2011), used by YIBs, show crop expansion while data from Ramankutty and Foley (1999) suggest reductions of the crop fraction over East China over the similar period. The role of land use change in our simulation might be conservative because we consider only land cover changes. Perturbed emissions from land use management, such as forest lodging, cropping practice, use of fertilizer, fire management and so on (Houghton, 2010) may alter regional carbon budget by changing carbon sinks to sources. Studies including gross emissions of land use perturbation estimated a global net land source to atmosphere, which shows decreasing trend in the last 3 decades (Ciais et al., 2013). Such change may help strengthen net land carbon sink but is missing in our study.

4.6 Impacts of biospheric changes

The land biosphere has experienced significant changes in the past 3 decades. At north of 30°N, changes in LAI account for 25% of the trends in regional carbon fluxes and isoprene emissions. However, the extension of growing season alone makes insignificant contributions to the increased carbon assimilation. This conclusion is inconsistent with

631 site-level observations that show evident increases in carbon assimilation at early spring
632 and/or late autumn in recent decades (Dragoni et al., 2011; Keenan et al., 2014). The
633 causes for such discrepancies lie in two. First, phenology at specific location may exhibit
634 much more intense changes than that at larger scale. For example, Dragoni et al. (2011)
635 estimated extensions of growing season by 2.3-3.3 day a^{-1} in Morgan-Monroe State
636 Forest in south-central Indiana of US for 1998-2008. The magnitude of this change is ~10
637 times larger than the observed value of 0.36 day a^{-1} from satellite and simulated value of
638 0.22 day a^{-1} with YIBs for the northern lands. Second, enhanced temperature also
639 contributes to the stronger uptake at early spring and late autumn. One difficulty for the
640 observation-based estimate of phenological impacts is that extension of growing season is
641 accompanied by warmer climate, which may stimulate both carbon assimilation and
642 BVOC production. In a recent study, Barlow et al. (2015) found invariant length of land
643 carbon uptake period at high northern latitudes based on the first time differential of
644 atmospheric CO_2 concentrations, suggesting that increased greenness is not necessarily
645 equal to enhanced carbon uptake in shoulder seasons. Furthermore, Barlow et al. (2015)
646 showed that enhanced peak uptake is the main driver for the strengthened carbon sink at
647 high northern latitudes over the past 4 decades. These conclusions are supportive of our
648 simulations for the monthly trends at subtropical regions (North America, Europe, and
649 East Asia) (Fig. S5).
650
651
652 **5 Conclusions**
653
654 With YIBs model, we estimated global increases of carbon assimilation especially at
655 tropical areas for 1982-2011. This trend is mainly attributed to the widespread CO_2
656 fertilization effect, and jointly affected by changes in meteorology and land cover.
657 Increase of temperature promotes carbon uptake of forest ecosystems at high latitudes
658 (>30°N) while drought tendency dampens GPP and NPP of grasslands and shrublands at
659 low latitudes (30°S-30°N). The widespread increases of LAI at northern lands account for
660 ~25% of the regional GPP trends. Significant changes in phenology are found at north of
661 30°N; however, this temperature-driven phenological change alone is not promoting

662 regional carbon assimilation. Changes in land use show limited influences on global
663 carbon fluxes, except for some regional impacts over Europe (afforestation) and China
664 (deforestation). Due to the simultaneous enhancement in soil respiration, land carbon sink
665 has remained almost stable in the past 3 decades. The YIBs model does not yet include a
666 fully coupled carbon-nitrogen cycle, thus the model may overestimate CO_2 fertilization
667 effects. On the contrary, implementation of drought-dependent phenology may amplify
668 drought inhibition effects on photosynthesis and result in an underestimation of carbon
669 uptake.
670
671 We estimated global trends of BVOC emissions with two schemes. Simulations with
672 PS_BVOC scheme show increasing isoprene emissions, mainly attributed to the increases
673 of temperature. For this scheme, CO_2 effects are neutralized due to both fertilization (on
674 photosynthesis) and inhibition (on isoprene). Simulations with MEGAN scheme show
675 decreasing emissions of isoprene and monoterpene because of CO_2 inhibition, especially
676 in the tropics. In subtropical areas, both schemes predict regional increases of BVOC
677 emissions in Europe following the warming trend and afforestation, but reductions in the
678 U.S. and China due to cropland expansion.
679
680
681 *Acknowledgements*. Funding support for this research is provided by the NASA
682 Atmospheric Composition Campaign Data Analysis and Modeling Program. This project
683 was supported in part by the facilities and staff of the Yale University Faculty of Arts and
684 Sciences High Performance Computing Center.
685
686

687 **References**

688 Ainsworth, E. A., and Long, S. P.: What have we learned from 15 years of free-air CO2
689 enrichment (FACE)? A meta-analytic review of the responses of photosynthesis,
690 canopy, New Phytol, 165, 351-371, doi:10.1111/J.1469-8137.2004.01224.X, 2005.
691 Arneth, A., Niinemets, U., Pressley, S., Back, J., Hari, P., Karl, T., Noe, S., Prentice, I.
692 C., Serca, D., Hickler, T., Wolf, A., and Smith, B.: Process-based estimates of
693 terrestrial ecosystem isoprene emissions: incorporating the effects of a direct CO2-
694 isoprene interaction, Atmos Chem Phys, 7, 31-53, doi:10.5194/acp-7-31-2007, 2007.
695 Barlow, J. M., Palmer, P. I., Bruhwiler, L. M., and and Tans, P.: Analysis of CO2 mole
696 fraction data: first evidence of large-scale changes in CO2 uptake at high northern
697 latitudes, Atmos. Chem. Phys. Discuss., 15, 7089-7139, doi:10.5194/acpd-15-7089-
698 2015, 2015.
699 Beer, C., Reichstein, M., Tomelleri, E., Ciais, P., Jung, M., Carvalhais, N., Rodenbeck,
700 C., Arain, M. A., Baldocchi, D., Bonan, G. B., Bondeau, A., Cescatti, A., Lasslop, G.,
701 Lindroth, A., Lomas, M., Luyssaert, S., Margolis, H., Oleson, K. W., Roupsard, O.,
702 Veenendaal, E., Viovy, N., Williams, C., Woodward, F. I., and Papale, D.: Terrestrial
703 Gross Carbon Dioxide Uptake: Global Distribution and Covariation with Climate,
704 Science, 329, 834-838, doi:10.1126/Science.1184984, 2010.
705 Buckley, P. T.: Isoprene emissions from a Florida scrub oak species grown in ambient
706 and elevated carbon dioxide, Atmos Environ, 35, 631-634, doi:10.1016/S1352-
707 2310(00)00332-0, 2001.
708 Buitenwerf, R., Rose, L., and Higgins, S. I.: Three decades of multi-dimensional change
709 in global leaf phenology, Nat Clim Change, 5, 364-368, 2015.
710 Carslaw, K. S., Boucher, O., Spracklen, D. V., Mann, G. W., Rae, J. G. L., Woodward,
711 S., and Kulmala, M.: A review of natural aerosol interactions and feedbacks within
712 the Earth system, Atmos. Chem. Phys., 10, 1701-1737, doi:10.5194/acp-10-1701-
713 2010, 2010.
714 Centritto, M., Brilli, F., Fodale, R., and Loreto, F.: Different sensitivity of isoprene
715 emission, respiration and photosynthesis to high growth temperature coupled with
716 drought stress in black poplar (Populus nigra) saplings, Tree Physiol, 31, 275-286,
717 doi:10.1093/Treephys/Tpq112, 2011.
718 Ciais, P., Sabine, C., Bala, G., Bopp, L., Brovkin, V., Canadell, J., Chhabra, A., DeFries,
719 R., Galloway, J., Heimann, M., Jones, C., Le Quere, C., Myneni, R., Piao, S., and
720 Thornton, P.: Carbon and other biogeochemical cycles, in: Climate Change 2013: The
721 Physical Science Basis. Contribution of Working Group I to the Fifth Assessment
722 Report of the Intergovernmental Panel on Climate Change, edited by: Stocker, T. F.,
723 Qin, D., Plattner, G.-K., Tignor, M., Allen, S. K., Boschung, J., Nauels, A., Xia, Y.,
724 Bex, V., and Midgley, P. M., Cambridge University Press, Cambridge, United
725 Kingdom and New York, NY, USA, 465-570, 2013.
726 Collatz, G. J., Ball, J. T., Grivet, C., and Berry, J. A.: Physiological and Environmental-
727 Regulation of Stomatal Conductance, Photosynthesis and Transpiration - a Model
728 That Includes a Laminar Boundary-Layer, Agr Forest Meteorol, 54, 107-136,
729 doi:10.1016/0168-1923(91)90002-8, 1991.
730 Cox, P. M.: Description of the "TRIFFID" Dynamic Global Vegetation Model, Hadley
731 Centre technical note 24, Berks, UK, 2001.

732 Defries, R. S., Hansen, M. C., Townshend, J. R. G., Janetos, A. C., and Loveland, T. R.:
733 A new global 1-km dataset of percentage tree cover derived from remote sensing,
734 Global Change Biol, 6, 247-254, doi:10.1046/J.1365-2486.2000.00296.X, 2000.
735 Dragoni, D., Schmid, H. P., Wayson, C. A., Potter, H., Grimmond, C. S. B., and
736 Randolph, J. C.: Evidence of increased net ecosystem productivity associated with a
737 longer vegetated season in a deciduous forest in south-central Indiana, USA, Global
738 Change Biol, 17, 886-897, doi:10.1111/J.1365-2486.2010.02281.X, 2011.
739 Farquhar, G. D., Caemmerer, S. V., and Berry, J. A.: A Biochemical-Model of
740 Photosynthetic Co2 Assimilation in Leaves of C-3 Species, Planta, 149, 78-90,
741 doi:10.1007/Bf00386231, 1980.
742 Guenther, A. B., Zimmerman, P. R., Harley, P. C., Monson, R. K., and Fall, R.: Isoprene
743 and Monoterpene Emission Rate Variability - Model Evaluations and Sensitivity
744 Analyses, J. Geophys. Res., 98, 12609-12617, doi:10.1029/93jd00527, 1993.
745 Guenther, A. B., Hewitt, C. N., Erickson, D., Fall, R., Geron, C., Graedel, T., Harley, P.,
746 Klinger, L., Lerdau, M., Mckay, W. A., Pierce, T., Scholes, B., Steinbrecher, R.,
747 Tallamraju, R., Taylor, J., and Zimmerman, P.: A Global-Model of Natural Volatile
748 Organic-Compound Emissions, J. Geophys. Res., 100, 8873-8892,
749 doi:10.1029/94jd02950, 1995.
750 Hansen, M. C., DeFries, R. S., Townshend, J. R. G., Carroll, M., Dimiceli, C., and
751 Sohlberg, R. A.: Global Percent Tree Cover at a Spatial Resolution of 500 Meters:
752 First Results of the MODIS Vegetation Continuous Fields Algorithm, Earth Interact,
753 7, 2003.
754 Heald, C. L., Wilkinson, M. J., Monson, R. K., Alo, C. A., Wang, G. L., and Guenther,
755 A.: Response of isoprene emission to ambient CO2 changes and implications for
756 global budgets, Global Change Biol, 15, 1127-1140, doi:10.1111/J.1365-
757 2486.2008.01802.X, 2009.
758 Heinsch, F. A., Zhao, M. S., Running, S. W., Kimball, J. S., Nemani, R. R., Davis, K. J.,
759 Bolstad, P. V., Cook, B. D., Desai, A. R., Ricciuto, D. M., Law, B. E., Oechel, W. C.,
760 Kwon, H., Luo, H. Y., Wofsy, S. C., Dunn, A. L., Munger, J. W., Baldocchi, D. D.,
761 Xu, L. K., Hollinger, D. Y., Richardson, A. D., Stoy, P. C., Siqueira, M. B. S.,
762 Monson, R. K., Burns, S. P., and Flanagan, L. B.: Evaluation of remote sensing based
763 terrestrial productivity from MODIS using regional tower eddy flux network
764 observations, Ieee T Geosci Remote, 44, 1908-1925, doi:10.1109/Tgrs.2005.853936,
765 2006.
766 Houghton, R. A.: How well do we know the flux of CO2 from land-use change?, Tellus
767 B, 62, 337-351, doi:Doi 10.1111/J.1600-0889.2010.00473.X, 2010.
768 Hurtt, G. C., Chini, L. P., Frolking, S., Betts, R. A., Feddema, J., Fischer, G., Fisk, J. P.,
769 Hibbard, K., Houghton, R. A., Janetos, A., Jones, C. D., Kindermann, G., Kinoshita,
770 T., Goldewijk, K. K., Riahi, K., Shevliakova, E., Smith, S., Stehfest, E., Thomson, A.,
771 Thornton, P., van Vuuren, D. P., and Wang, Y. P.: Harmonization of land-use
772 scenarios for the period 1500-2100: 600 years of global gridded annual land-use
773 transitions, wood harvest, and resulting secondary lands, Climatic Change, 109, 117-
774 161, doi:10.1007/S10584-011-0153-2, 2011.
775 Jeong, S. J., Ho, C. H., Gim, H. J., and Brown, M. E.: Phenology shifts at start vs. end of
776 growing season in temperate vegetation over the Northern Hemisphere for the period

1982-2008, Global Change Biol, 17, 2385-2399, doi:10.1111/J.1365-2486.2011.02397.X, 2011.
Jung, M., Reichstein, M., and Bondeau, A.: Towards global empirical upscaling of FLUXNET eddy covariance observations: validation of a model tree ensemble approach using a biosphere model, Biogeosciences, 6, 2001-2013, doi:10.5194/bg-6-2001-2009, 2009.
Keenan, T. F., Gray, J., Friedl, M. A., Toomey, M., Bohrer, G., Hollinger, D. Y., Munger, J. W., O'Keefe, J., Schmid, H. P., SueWing, I., Yang, B., and Richardson, A. D.: Net carbon uptake has increased through warming-induced changes in temperate forest phenology, Nat Clim Change, 4, 598-604, doi:10.1038/Nclimate2253, 2014.
Kivimaenpaa, M., Riikonen, J., Ahonen, V., Tervahauta, A., and Holopainen, T.: Sensitivity of Norway spruce physiology and terpenoid emission dynamics to elevated ozone and elevated temperature under open-field exposure, Environ Exp Bot, 90, 32-42, doi:10.1016/J.Envexpbot.2012.1t004, 2013.
Lathiere, J., Hauglustaine, D. A., Friend, A. D., De Noblet-Ducoudre, N., Viovy, N., and Folberth, G. A.: Impact of climate variability and land use changes on global biogenic volatile organic compound emissions, Atmos Chem Phys, 6, 2129-2146, doi:10.5194/acp-6-2129- 2006, 2006.
Le Quere, C., Raupach, M. R., Canadell, J. G., Marland, G., Bopp, L., Ciais, P., Conway, T. J., Doney, S. C., Feely, R. A., Foster, P., Friedlingstein, P., Gurney, K., Houghton, R. A., House, J. I., Huntingford, C., Levy, P. E., Lomas, M. R., Majkut, J., Metzl, N., Ometto, J. P., Peters, G. P., Prentice, I. C., Randerson, J. T., Running, S. W., Sarmiento, J. L., Schuster, U., Sitch, S., Takahashi, T., Viovy, N., van der Werf, G. R., and Woodward, F. I.: Trends in the sources and sinks of carbon dioxide, Nat Geosci, 2, 831-836, doi:10.1038/Ngeo689, 2009.
Li, Z. R., Ratliff, E. A., and Sharkey, T. D.: Effect of Temperature on Postillumination Isoprene Emission in Oak and Poplar, Plant Physiol, 155, 1037-1046, doi:10.1104/Pp.110.167551, 2011.
Liang, J. Y., Xia, J. Y., Liu, L. L., and Wan, S. Q.: Global patterns of the responses of leaf-level photosynthesis and respiration in terrestrial plants to experimental warming, J Plant Ecol, 6, 437-447, doi:10.1093/Jpe/Rtt003, 2013.
Mao, J. F., Shi, X. Y., Thornton, P. E., Hoffman, F. M., Zhu, Z. C., and Myneni, R. B.: Global Latitudinal-Asymmetric Vegetation Growth Trends and Their Driving Mechanisms: 1982-2009, Remote Sens, 5, 1484-1497, doi:Doi 10.3390/Rs5031484, 2013.
Marais, E. A., Jacob, D. J., Kurosu, T. P., Chance, K., Murphy, J. G., Reeves, C., Mills, G., Casadio, S., Millet, D. B., Barkley, M. P., Paulot, F., and Mao, J.: Isoprene emissions in Africa inferred from OMI observations of formaldehyde columns, Atmos Chem Phys, 12, 6219-6235, doi:10.5194/Acp-12-6219-2012, 2012.
Meinshausen, M., Smith, S. J., Calvin, K., Daniel, J. S., Kainuma, M. L. T., Lamarque, J. F., Matsumoto, K., Montzka, S. A., Raper, S. C. B., Riahi, K., Thomson, A., Velders, G. J. M., and van Vuuren, D. P. P.: The RCP greenhouse gas concentrations and their extensions from 1765 to 2300, Climatic Change, 109, 213-241, doi:10.1007/S10584-011-0156-Z, 2011.
Monson, R. K., Trahan, N., Rosenstiel, T. N., Veres, P., Moore, D., Wilkinson, M., Norby, R. J., Volder, A., Tjoelker, M. G., Briske, D. D., Karnosky, D. F., and Fall,

R.: Isoprene emission from terrestrial ecosystems in response to global change: minding the gap between models and observations, Philos T R Soc A, 365, 1677-1695, doi:10.1098/Rsta.2007.2038, 2007.

Muller, J. F., Stavrakou, T., Wallens, S., De Smedt, I., Van Roozendael, M., Potosnak, M. J., Rinne, J., Munger, B., Goldstein, A., and Guenther, A. B.: Global isoprene emissions estimated using MEGAN, ECMWF analyses and a detailed canopy environment model, Atmos Chem Phys, 8, 1329-1341, 2008.

Naik, V., Delire, C., and Wuebbles, D. J.: Sensitivity of global biogenic isoprenoid emissions to climate variability and atmospheric CO2, J. Geophys. Res., 109, D06301, doi:10.1029/2003jd004236, 2004.

Niinemets, U., and Sun, Z. H.: How light, temperature, and measurement and growth [CO2] interactively control isoprene emission in hybrid aspen, J Exp Bot, 66, 841-851, doi:10.1093/Jxb/Eru443, 2015.

Norby, R. J., DeLucia, E. H., Gielen, B., Calfapietra, C., Giardina, C. P., King, J. S., Ledford, J., McCarthy, H. R., Moore, D. J. P., Ceulemans, R., De Angelis, P., Finzi, A. C., Karnosky, D. F., Kubiske, M. E., Lukac, M., Pregitzer, K. S., Scarascia-Mugnozza, G. E., Schlesinger, W. H., and Oren, R.: Forest response to elevated CO2 is conserved across a broad range of productivity, P Natl Acad Sci USA, 102, 18052-18056, doi:10.1073/Pnas.0509478102, 2005.

Oleson, K. W., Lawrence, D. M., Bonan, G. B., Drewniak, B., Huang, M., Koven, C. D., Levis, S., Li, F., Riley, W. J., Subin, Z. M., Swenson, S. C., Thornton, P. E., Bozbiyik, A., Fisher, R., Heald, C. L., Kluzek, E., Lamarque, J.-F., Lawrence, P. J., Leung, L. R., Lipscomb, W., Muszala, S., Ricciuto, D. M., Sacks, W., Sun, Y., Tang, J., and Yang, Z.-L.: Technical Description of version 4.5 of the Community Land Model (CLM), National Center for Atmospheric Research, Boulder, CONCAR Technical Note NCAR/TN-478+STR, 434, 2013.

Palmer, P. I., Abbot, D. S., Fu, T. M., Jacob, D. J., Chance, K., Kurosu, T. P., Guenther, A., Wiedinmyer, C., Stanton, J. C., Pilling, M. J., Pressley, S. N., Lamb, B., and Sumner, A. L.: Quantifying the seasonal and interannual variability of North American isoprene emissions using satellite observations of the formaldehyde column, J Geophys Res-Atmos, 111, D12315, doi:10.1029/2005jd006689, 2006.

Pan, Y. D., Birdsey, R. A., Fang, J. Y., Houghton, R., Kauppi, P. E., Kurz, W. A., Phillips, O. L., Shvidenko, A., Lewis, S. L., Canadell, J. G., Ciais, P., Jackson, R. B., Pacala, S. W., McGuire, A. D., Piao, S. L., Rautiainen, A., Sitch, S., and Hayes, D.: A Large and Persistent Carbon Sink in the World's Forests, Science, 333, 988-993, doi:10.1126/Science.1201609, 2011.

Pegoraro, E., Rey, A., Abrell, L., Vanharen, J., and Lin, G. H.: Drought effect on isoprene production and consumption in Biosphere 2 tropical rainforest, Global Change Biol, 12, 456-469, doi:Doi 10.1111/J.1365-2486.2006.01112.X, 2006.

Piao, S. L., Friedlingstein, P., Ciais, P., Viovy, N., and Demarty, J.: Growing season extension and its impact on terrestrial carbon cycle in the Northern Hemisphere over the past 2 decades, Global Biogeochem Cy, 21, Gb3018, doi:10.1029/2006gb002888, 2007.

Piao, S. L., Sitch, S., Ciais, P., Friedlingstein, P., Peylin, P., Wang, X. H., Ahlstrom, A., Anav, A., Canadell, J. G., Cong, N., Huntingford, C., Jung, M., Levis, S., Levy, P. E., Li, J. S., Lin, X., Lomas, M. R., Lu, M., Luo, Y. Q., Ma, Y. C., Myneni, R. B.,

869 Poulter, B., Sun, Z. Z., Wang, T., Viovy, N., Zaehle, S., and Zeng, N.: Evaluation of
870 terrestrial carbon cycle models for their response to climate variability and to CO2
871 trends, Global Change Biol, 19, 2117-2132, doi:10.1111/Gcb.12187, 2013.
872 Possell, M., Hewitt, C. N., and Beerling, D. J.: The effects of glacial atmospheric CO2
873 concentrations and climate on isoprene emissions by vascular plants, Global Change
874 Biol, 11, 60-69, doi:10.1111/J.1365-2486.2004.00889.X, 2005.
875 Ramankutty, N., and Foley, J. A.: Estimating historical changes in global land cover:
876 Croplands from 1700 to 1992, Global Biogeochem Cy, 13, 997-1027,
877 doi:10.1029/1999gb900046, 1999.
878 Richardson, A. D., Hollinger, D. Y., Dail, D. B., Lee, J. T., Munger, J. W., and O'Keefe,
879 J.: Influence of spring phenology on seasonal and annual carbon balance in two
880 contrasting New England forests, Tree Physiol, 29, 321-331, doi:Doi
881 10.1093/Treephys/Tpn040, 2009.
882 Richardson, A. D., Keenan, T. F., Migliavacca, M., Ryu, Y., Sonnentag, O., and Toomey,
883 M.: Climate change, phenology, and phenological control of vegetation feedbacks to
884 the climate system, Agr Forest Meteorol, 169, 156-173, 2013.
885 Ruehr, N. K., Martin, J. G., and Law, B. E.: Effects of water availability on carbon and
886 water exchange in a young ponderosa pine forest: Above- and belowground
887 responses, Agr Forest Meteorol, 164, 136-148, doi:10.1016/J.Agrformet.2012.05.015,
888 2012.
889 Sarmiento, J. L., Gloor, M., Gruber, N., Beaulieu, C., Jacobson, A. R., Fletcher, S. E. M.,
890 Pacala, S., and Rodgers, K.: Trends and regional distributions of land and ocean
891 carbon sinks, Biogeosciences, 7, 2351-2367, doi:10.5194/Bg-7-2351-2010, 2010.
892 Schaefer, K., Collatz, G. J., Tans, P., Denning, A. S., Baker, I., Berry, J., Prihodko, L.,
893 Suits, N., and Philpott, A.: Combined Simple Biosphere/Carnegie-Ames-Stanford
894 Approach terrestrial carbon cycle model, J. Geophys. Res., 113, G03034,
895 doi:10.1029/2007jg000603, 2008.
896 Scott, C. E., Rap, A., Spracklen, D. V., Forster, P. M., Carslaw, K. S., Mann, G. W.,
897 Pringle, K. J., Kivekas, N., Kulmala, M., Lihavainen, H., and Tunved, P.: The direct
898 and indirect radiative effects of biogenic secondary organic aerosol, Atmos Chem
899 Phys, 14, 447-470, doi:10.5194/Acp-14-447-2014, 2014.
900 Sindelarova, K., Granier, C., Bouarar, I., Guenther, A., Tilmes, S., Stavrakou, T., Muller,
901 J. F., Kuhn, U., Stefani, P., and Knorr, W.: Global data set of biogenic VOC
902 emissions calculated by the MEGAN model over the last 30 years, Atmos Chem
903 Phys, 14, 9317-9341, doi:10.5194/Acp-14-9317-2014, 2014.
904 Sitch, S., Friedlingstein, P., Gruber, N., Jones, S. D., Murray-Tortarolo, G., Ahlström, A.,
905 Doney, S. C., Graven, H., Heinze, C., Huntingford, C., Levis, S., Levy, P. E., Lomas,
906 M., Poulter, B., Viovy, N., Zaehle, S., Zeng, N., Arneth, A., Bonan, G., Bopp, L.,
907 Canadell, J. G., Chevallier, F., Ciais, P., Ellis, R., Gloor, M., Peylin, P., Piao, S. L.,
908 Quéré, C. L., Smith, B., Zhu, Z., and Myneni, R.: Recent trends and drivers of
909 regional sources and sinks of carbon dioxide, Biogeosciences, 12, 653-679, 2015.
910 Stavrakou, T., Muller, J. F., Bauwens, M., De Smedt, I., Van Roozendael, M., Guenther,
911 A., Wild, M., and Xia, X.: Isoprene emissions over Asia 1979-2012: impact of
912 climate and land-use changes, Atmos Chem Phys, 14, 4587-4605, doi:10.5194/Acp-
913 14-4587-2014, 2014.

914 Sun, Z. H., Hve, K., Vislap, V., and Niinemets, U.: Elevated [CO2] magnifies isoprene
915 emissions under heat and improves thermal resistance in hybrid aspen, J Exp Bot, 64,
916 5509-5523, doi:10.1093/Jxb/Ert318, 2013.
917 Unger, N., Harper, K., Zheng, Y., Kiang, N. Y., Aleinov, I., Arneth, A., Schurgers, G.,
918 Amelynck, C., Goldstein, A., Guenther, A., Heinesch, B., Hewitt, C. N., Karl, T.,
919 Laffineur, Q., Langford, B., McKinney, K. A., Misztal, P., Potosnak, M., Rinne, J.,
920 Pressley, S., Schoon, N., and Serça, D.: Photosynthesis-dependent isoprene emission
921 from leaf to planet in a global carbon–chemistry–climate model, Atmos. Chem. Phys.,
922 13, 17717-17791, doi:10.5194/acp-13-10243-2013, 2013.
923 Unger, N.: On the role of plant volatiles in anthropogenic global climate change,
924 Geophys Res Lett, 41, 8563-8569, doi:10.1002/2014gl061616, 2014.
925 Uppala, S. M., Kallberg, P. W., Simmons, A. J., Andrae, U., Bechtold, V. D., Fiorino,
926 M., Gibson, J. K., Haseler, J., Hernandez, A., Kelly, G. A., Li, X., Onogi, K.,
927 Saarinen, S., Sokka, N., Allan, R. P., Andersson, E., Arpe, K., Balmaseda, M. A.,
928 Beljaars, A. C. M., Van De Berg, L., Bidlot, J., Bormann, N., Caires, S., Chevallier,
929 F., Dethof, A., Dragosavac, M., Fisher, M., Fuentes, M., Hagemann, S., Holm, E.,
930 Hoskins, B. J., Isaksen, L., Janssen, P. A. E. M., Jenne, R., McNally, A. P., Mahfouf,
931 J. F., Morcrette, J. J., Rayner, N. A., Saunders, R. W., Simon, P., Sterl, A., Trenberth,
932 K. E., Untch, A., Vasiljevic, D., Viterbo, P., and Woollen, J.: The ERA-40 re-
933 analysis, Q J Roy Meteor Soc, 131, 2961-3012, doi:10.1256/Qj.04.176, 2005.
934 von Caemmerer, S., and Farquhar, G. D.: Some Relationships between the Biochemistry
935 of Photosynthesis and the Gas-Exchange of Leaves, Planta, 153, 376-387, 1981.
936 Weedon, G. P., Gomes, S., Viterbo, P., Shuttleworth, W. J., Blyth, E., Osterle, H., Adam,
937 J. C., Bellouin, N., Boucher, O., and Best, M.: Creation of the WATCH Forcing Data
938 and Its Use to Assess Global and Regional Reference Crop Evaporation over Land
939 during the Twentieth Century, J Hydrometeorol, 12, 823-848,
940 doi:10.1175/2011jhm1369.1, 2011.
941 Weedon, G. P., Balsamo, G., Bellouin, N., Gomes, S., Best, M. J., and Viterbo, P.: The
942 WFDEI meteorological forcing data set: WATCH Forcing Data methodology applied
943 to ERA-Interim reanalysis data, Water Resources Research, 2014.
944 Wofsy, S. C., Goulden, M. L., Munger, J. W., Fan, S. M., Bakwin, P. S., Daube, B. C.,
945 Bassow, S. L., and Bazzaz, F. A.: Net Exchange of Co2 in a Midlatitude Forest,
946 Science, 260, 1314-1317, doi:10.1126/Science.260.5112.1314, 1993.
947 Wu, Z. T., Dijkstra, P., Koch, G. W., Penuelas, J., and Hungate, B. A.: Responses of
948 terrestrial ecosystems to temperature and precipitation change: a meta-analysis of
949 experimental manipulation, Global Change Biol, 17, 927-942, doi:10.1111/J.1365-
950 2486.2010.02302.X, 2011.
951 Xia, J. B., Zhang, G. C., Wang, R. R., and Zhang, S. Y.: Effect of soil water availability
952 on photosynthesis in Ziziphus jujuba var. spinosus in a sand habitat formed from
953 seashells: Comparison of four models, Photosynthetica, 52, 253-261, doi:Doi
954 10.1007/S11099-014-0030-0, 2014.
955 Yue, X., and Unger, N.: Ozone vegetation damage effects on gross primary productivity
956 in the United States, Atmos. Chem. Phys., 14, 9137-9153, doi:10.5194/acp-14-9137-
957 2014, 2014.

Yue, X., and Unger, N.: The Yale Interactive terrestrial Biosphere model: description, evaluation and implementation into NASA GISS ModelE2, Geosci. Model Dev., 8, 2399-2417, doi:10.5194/gmd-8-2399-2015, 2015.

Yue, X., Unger, N., Keenan, T. F., Zhang, X., and Vogel, C. S.: Probing the past 30-year phenology trend of U.S. deciduous forests, Biogeosciences, 12, 4693-4709, doi:10.5194/bg-12-4693-2015, 2015.

Zhao, M. S., Heinsch, F. A., Nemani, R. R., and Running, S. W.: Improvements of the MODIS terrestrial gross and net primary production global data set, Remote Sens Environ, 95, 164-176, doi:10.1016/J.Rse.2004.12.011, 2005.

Zhao, M. S., and Running, S. W.: Drought-Induced Reduction in Global Terrestrial Net Primary Production from 2000 Through 2009, Science, 329, 940-943, doi:10.1126/Science.1192666, 2010.

Zheng, Y., Unger, N., Barley, M., and Yue, X.: Relationships between photosynthesis and formaldehyde as a probe of isoprene emission, Atmos. Chem. Phys. , 15, 8559-8576, doi:10.5194/acp-15-8559-2015, 2015.

Zhu, Z. C., Bi, J., Pan, Y. Z., Ganguly, S., Anav, A., Xu, L., Samanta, A., Piao, S. L., Nemani, R. R., and Myneni, R. B.: Global Data Sets of Vegetation Leaf Area Index (LAI)3g and Fraction of Photosynthetically Active Radiation (FPAR)3g Derived from Global Inventory Modeling and Mapping Studies (GIMMS) Normalized Difference Vegetation Index (NDVI3g) for the Period 1981 to 2011, Remote Sens, 5, 927-948, doi:10.3390/Rs5020927, 2013.

981
982
983 **Table 1.** Summary of model simulations driven with WFDEI reanalysis.
984

Simulations	Descriptions
CO2_MET_LUC	Annually updated [CO_2] and land cover, and hourly meteorology. All forcings vary for 1980-2011.
CO2_MET	Annually updated [CO_2] and hourly meteorology for 1980-2011, land cover is prescribed at the year 1980.
CO2_ONLY	Annually updated [CO_2] for 1980-2011, land cover is prescribed and hourly meteorology is recycled for the year 1980.
MET_ONLY	Hourly meteorology varies for 1980-2011. [CO_2] and land cover are prescribed at the year 1980.
LUC_ONLY	Annually updated land cover for 1980-2011, [CO_2] is prescribed and hourly meteorology is recycled for the year 1980.
TEMP_ONLY	Hourly temperature for 1980-2011 but other meteorological variables are recycled for 1980. [CO_2] and land cover are prescribed at the year 1980.
PAR_ONLY	Hourly PAR for 1980-2011 but other meteorological variables are recycled for 1980. [CO_2] and land cover are prescribed at the year 1980.
SOILW_ONLY	Hourly soil wetness for 1980-2011 but other meteorological variables are recycled for 1980. [CO_2] and land cover are prescribed at the year 1980.
LAI_ONLY	Hourly meteorology is recycled for the year 1980. [CO_2] and land cover are prescribed at the year 1980. Leaf area index varies for 1980-2011.
PHEN_ONLY	Hourly meteorology is recycled for the year 1980. [CO_2] and land cover are prescribed at the year 1980. Phenology varies for 1980-2011.

985
986
987
988
989
990

991
992
993
994 **Table 2.** Summary of trends in different domains from the simulation CO2_MET_LUC,
995 which is driven with WFDEI meteorology. Significant trends ($p < 0.05$) are indicated
996 with asterisks.
997

Regions	Amazon	North America	Central Africa	Europe	East Asia	Indonesia
LAI (10^{-3} m^2 m^{-2} a^{-1})	0.8	0.4 *	1.8 *	3.5 *	-0.4 *	-0.1
GPP (Tg C a^{-2})	52.7 *	13.6	83.3 *	53.4 *	42.4 *	15.3 *
NPP (Tg C a^{-2})	27.1 *	9.7	51.7 *	33.2 *	27.2 *	11.4 *
NEP (Tg C a^{-2})	-8.1	-1.7	11.6	6.7	-6.2	0.2
Ra (Tg C a^{-2})	25.6 *	3.9	31.6 *	20.2 *	15.2 *	3.9 *
Rh (Tg C a^{-2})	35.2 *	11.2 *	39.8 *	26.6 *	33.4 *	11.2 *
Isoprene PS_BVOC (Tg C a^{-2})	0.04	-0.03	0.25 *	0.16 *	-0.02	-0.01
Isoprene MEGAN (Tg C a^{-2})	-0.43 *	-0.07 *	-0.14 *	0.10 *	-0.13 *	-0.16 *
Monoterpene (Tg C a^{-2})	-0.03 *	0.01	-0.002	0.03 *	-0.02 *	-0.02 *
Budburst (days a^{-1})	N/A [a]	-0.01	N/A	-0.16 *	-0.15 *	N/A
Dormancy onset (days a^{-1})	N/A	0.09 *	N/A	0.16 *	0.03	N/A
Season extension (days a^{-1})	N/A	0.1 *	N/A	0.32 *	0.18 *	N/A

998
999
1000 [a] Phenology is set to constant for tropical rainforest in the model.

Table 3. Summary of simulated trends of global carbon fluxes (Tg C a^{-2}) from different experiments. Simulations are using WFDEI meteorology. Significant trends ($p < 0.05$) are indicated with asterisks.

Simulations	GPP	NPP	NEP	Ra	Rh
CO2_MET_LUC	297.4 *	185.3 *	2.7	112.1 *	180.9 *
CO2_MET	329.5 *	206.2 *	4.5	123.3 *	199.8 *
CO2_ONLY	412.4 *	299 *	66.2 *	113.5 *	231.9 *
MET_ONLY	-108.6 *	-108.2 *	-72.6 *	-0.4	-35
LUC_ONLY	-13 *	-8 *	-34.6 *	-5 *	26.9 *
TEMP_ONLY	-23.2 *	-56 *	-10.2 *	32.8 *	-43.6 *
PAR_ONLY	-5.9	-5.8	-23.4 *	-0.1	18.3 *
SOILW_ONLY	-84.8 *	-51 *	-13.1 *	-33.8 *	-38.3
LAI_ONLY	-8.8	-25.6 *	-44.5 *	16.7 *	18.7 *
PHEN_ONLY	-103.1 *	-56.2 *	47.1 *	-46.8 *	-102.9 *

Figure Captions

Figure 1. Comparison of trends in (b-f) simulated leaf area index (LAI) with (a) observations for 1982-2011. Observations are derived from GIMMS NDVI. Simulations are performed with either (d, e, f) single forcings or (b, c) the combinations of these forcings. Forcings considered include meteorology from WFDEI reanalysis (MET), CO_2 fertilization (CO2), and land use change (LUC). For every forcing included in the simulation, the year-to-year fields are utilized. Otherwise, the forcing is prescribed at the year 1980. Only significant trends ($p < 0.05$) are presented. The six box regions in (a) indicate areas for statistical analyses in Table 2.

Figure 2. Simulated trends in (a) gross primary productivity (GPP), (c) net primary productivity (NPP), and (e) net ecosystem productivity (NEP), and (b, d, f) the dominant drivers for these changes during 1982-2011. Simulations are performed with WFDEI reanalysis. Three factors, meteorological forcing, CO_2 fertilization, and land use change, are considered as the potential drivers of flux trends. For each grid in figures (b, d, f), the factor generating the largest (either maximum or minimum) trend with the same sign as the net change (a, c, e) is selected as the driving factor. Only significant trends ($p < 0.05$) are presented.

Figure 3. Comparisons of trends in (a, b) GPP and (c, d) NPP for 2000-2011 between (a, c) simulations and (b, d) observations. Observed fluxes are retrieved from the Moderate Resolution Imaging Spectroradiometer (MODIS).

Figure 4. Simulated (a) trends in GPP driven alone with WFDEI reanalysis and the (b) drivers for such changes. Simulation in (a) is performed with year-to-year meteorological forcings but prescribed [CO_2] and land use in the year 1980. Simulations in (b) are the same as (a) except that the year-to-year variations are allowed only for a single meteorological variable (temperature, PAR, or soil wetness) each time. For each grid, the meteorological variable generating the largest (either maximum or minimum) trend with

1040 the same sign as the net change (a) is selected as the driving factor. Only significant
1041 trends ($p < 0.05$) are presented.
1042
1043 **Figure 5.** Global total fluxes of GPP, NPP, Rh (heterotrophic respiration), and NEP from
1044 different sensitivity simulations with all forcings (black), meteorology alone (red), CO_2
1045 alone (green), and land use change alone (blue).
1046
1047 **Figure 6.** Simulated trends of (a, c) isoprene and (e) monoterpene, and (b, d, f) the
1048 dominant drivers for these changes during 1982-2011. Simulations are performed with
1049 WFDEI reanalysis. Isoprene emissions are simulated with (a) PS_BVOC and (c)
1050 MEGAN schemes. Three factors, meteorological forcing, CO_2 effects (both fertilization
1051 and inhibition), and land use change, are considered as the potential drivers of flux
1052 trends. For each grid in figures (b, d, f), the factor generating the largest (either maximum
1053 or minimum) trend with the same sign as the net change (a-c) is selected as the driving
1054 factor. Only significant trends ($p < 0.05$) are presented.
1055
1056 **Figure 7.** Responses of (a) GPP and (b) isoprene emissions to the changes in the annual
1057 average LAI at the north of 30°N for simulations CO2_MET (red) and LAI_ONLY
1058 (blue). Both GPP and isoprene emissions are the sum of all PFTs. Isoprene is simulated
1059 with the PS_BVOC scheme. Units of trends are (a) Pg C a^{-1} LAI^{-1} and (b) Tg C a^{-1} LAI^{-1}.
1060 The spatial distribution of GPP and isoprene changes is shown in Figure S2.
1061
1062 **Figure 8.** Predicted trend in (a) budburst and (b) dormancy onset dates over north of
1063 30°N and the responses of (c) GPP and (d) isoprene emissions to the changes in the
1064 growing length. Both GPP and isoprene emissions are the sum of DBF, shrub, grassland,
1065 and tundra. Isoprene is simulated with the PS_BVOC scheme. For the bottom panel,
1066 different colors indicate sensitivity experiments with different year-to-year forcings: CO_2
1067 and meteorology (red), temperature only (magenta), and phenology only (blue). Units of
1068 trends are (a) day a^{-1}, (b) day a^{-1}, (c) Pg C a^{-1} day^{-1}, and (d) Tg C a^{-1} day^{-1}. The spatial
1069 distribution of GPP and isoprene changes is shown in Figure S2.
1070

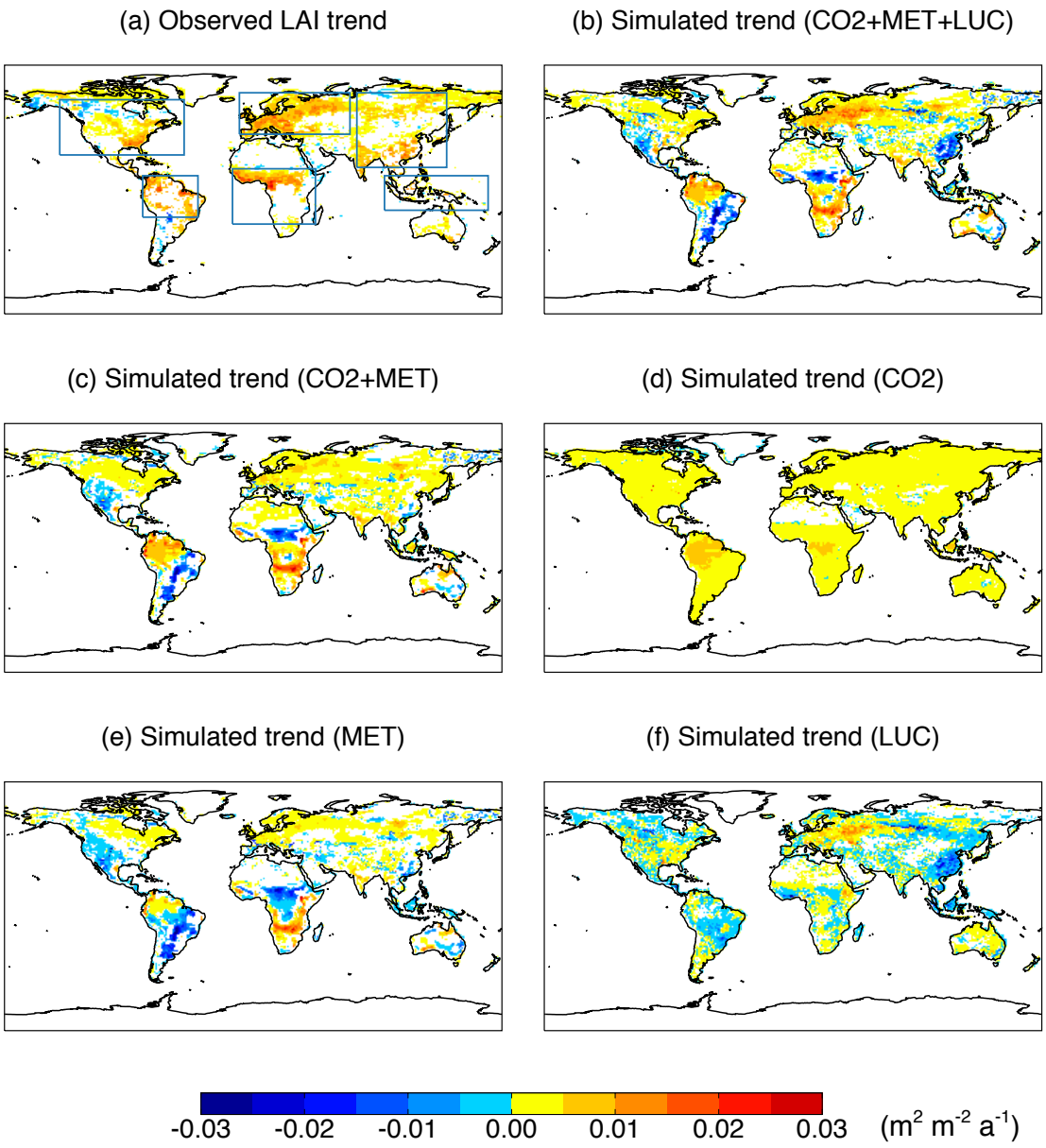

Figure 1. Comparison of trends in (b-f) simulated leaf area index (LAI) with (a) observations for 1982-2011. Observations are derived from GIMMS NDVI. Simulations are performed with either (d, e, f) single forcings or (b, c) the combinations of these forcings. Forcings considered include meteorology from WFDEI reanalysis (MET), CO_2 fertilization (CO2), and land use change (LUC). For every forcing included in the simulation, the year-to-year fields are utilized. Otherwise, the forcing is prescribed at the year 1980. Only significant trends ($p < 0.05$) are presented. The six box regions in (a) indicate areas for statistical analyses in Table 2.

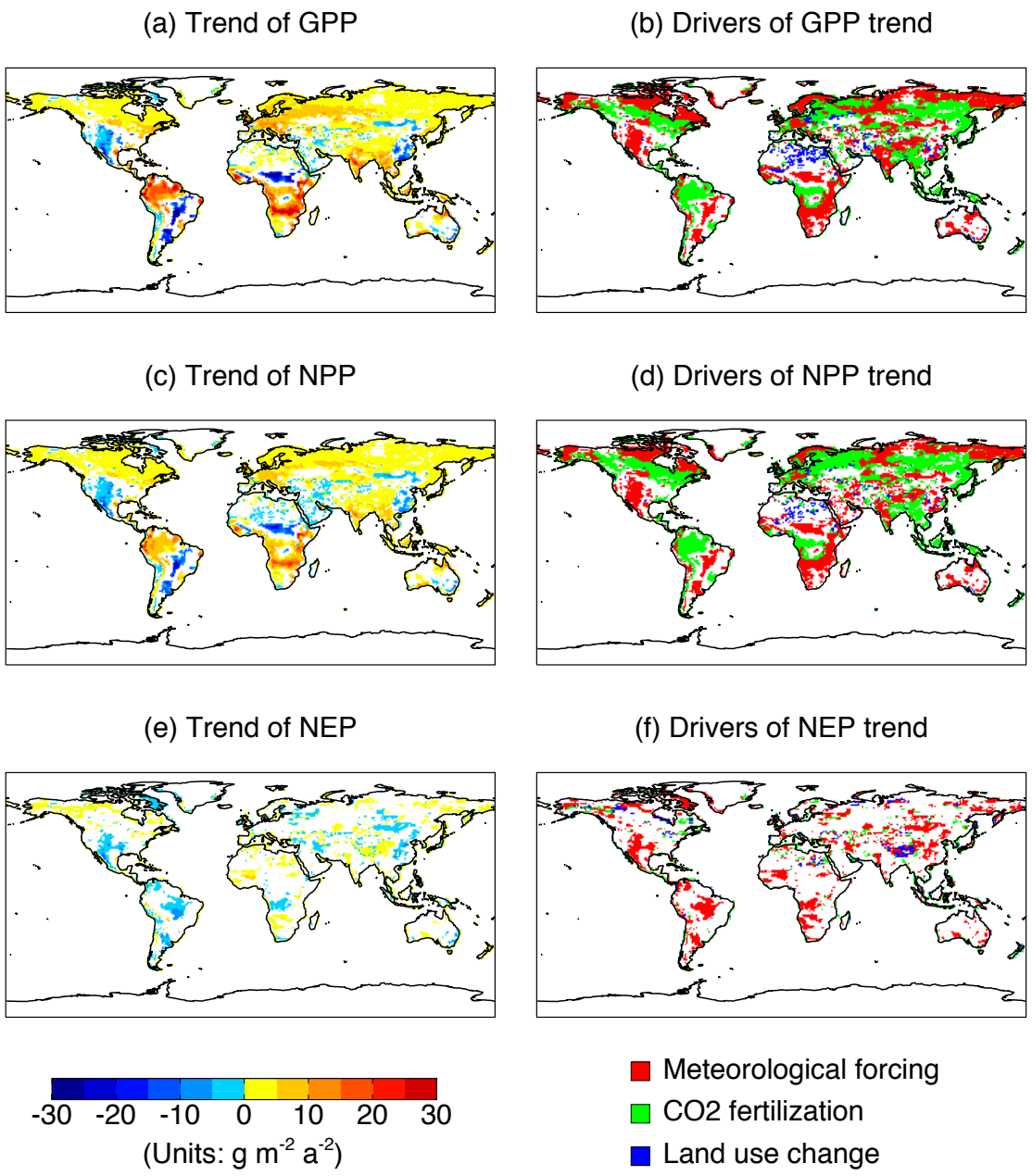

Figure 2. Simulated trends in (a) gross primary productivity (GPP), (c) net primary productivity (NPP), and (e) net ecosystem productivity (NEP), and (b, d, f) the dominant drivers for these changes during 1982-2011. Simulations are performed with WFDEI reanalysis. Three factors, meteorological forcing, CO_2 fertilization, and land use change, are considered as the potential drivers of flux trends. For each grid in figures (b, d, f), the factor generating the largest (either maximum or minimum) trend with the same sign as the net change (a, c, e) is selected as the driving factor. Only significant trends ($p < 0.05$) are presented.

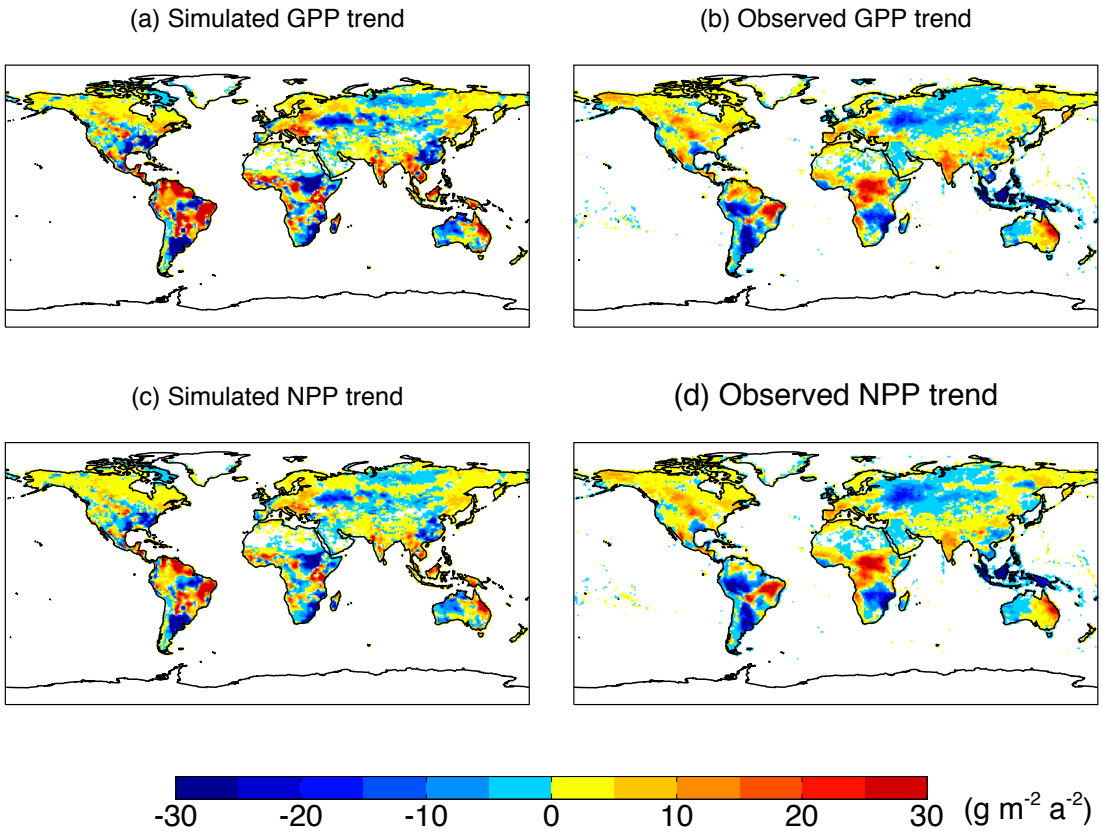

Figure 3. Comparisons of trends in (a, b) GPP and (c, d) NPP for 2000-2011 between (a, c) simulations and (b, d) observations. Observed fluxes are retrieved from the Moderate Resolution Imaging Spectroradiometer (MODIS).

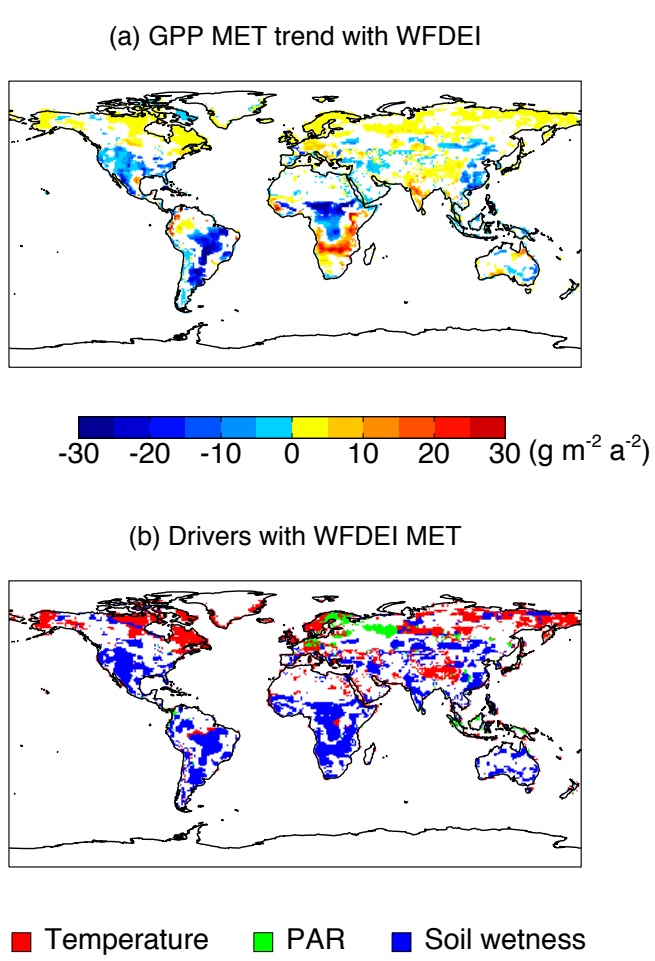

Figure 4. Simulated (a) trends in GPP driven alone with WFDEI reanalysis and the (b) drivers for such changes. Simulation in (a) is performed with year-to-year meteorological forcings but prescribed [CO_2] and land use in the year 1980. Simulations in (b) are the same as (a) except that the year-to-year variations are allowed only for a single meteorological variable (temperature, PAR, or soil wetness) each time. For each grid, the meteorological variable generating the largest (either maximum or minimum) trend with the same sign as the net change (a) is selected as the driving factor. Only significant trends ($p < 0.05$) are presented.

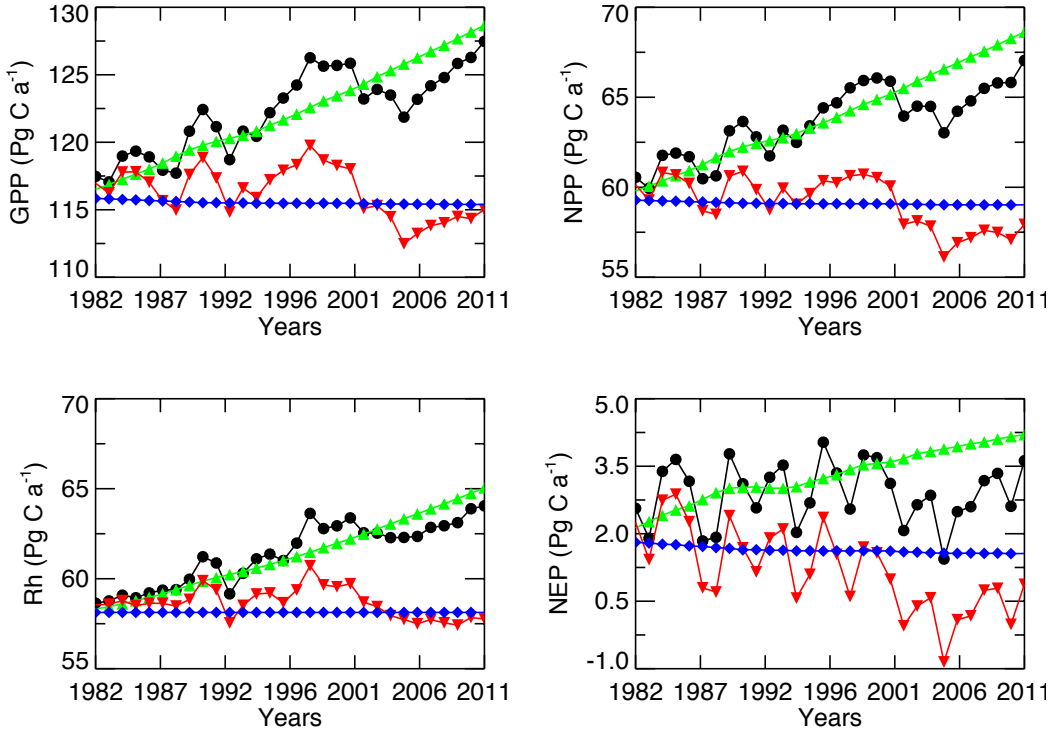

Figure 5. Global total fluxes of GPP, NPP, Rh (heterotrophic respiration), and NEP from different sensitivity simulations with all forcings (black), meteorology alone (red), CO_2 alone (green), and land use change alone (blue).

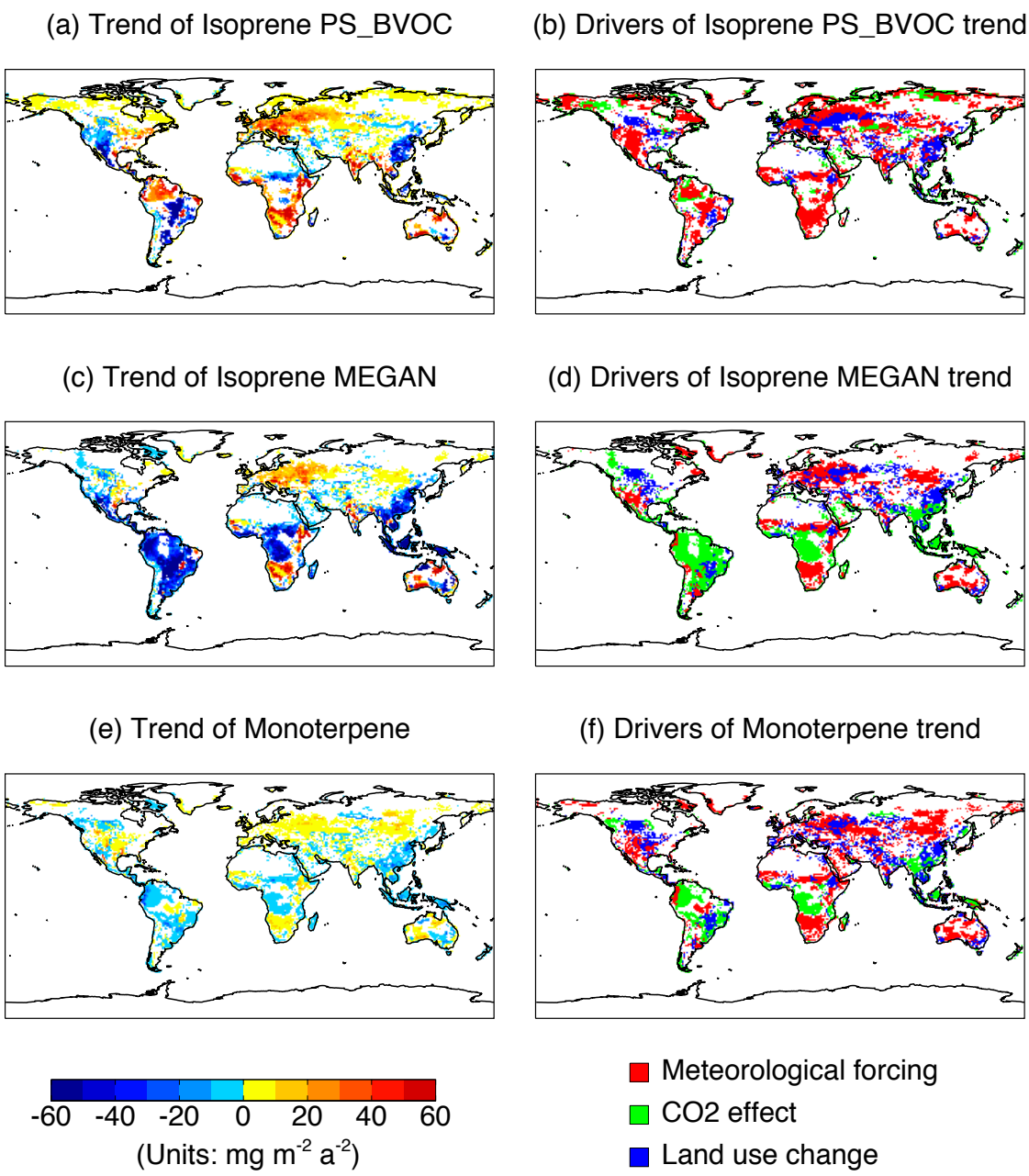

Figure 6. Simulated trends of (a, c) isoprene and (e) monoterpene, and (b, d, f) the dominant drivers for these changes during 1982-2011. Simulations are performed with WFDEI reanalysis. Isoprene emissions are simulated with (a) PS_BVOC and (c) MEGAN schemes. Three factors, meteorological forcing, CO_2 effects (both fertilization and inhibition), and land use change, are considered as the potential drivers of flux trends. For each grid in figures (b, d, f), the factor generating the largest (either maximum or minimum) trend with the same sign as the net change (a-c) is selected as the driving factor. Only significant trends ($p < 0.05$) are presented.

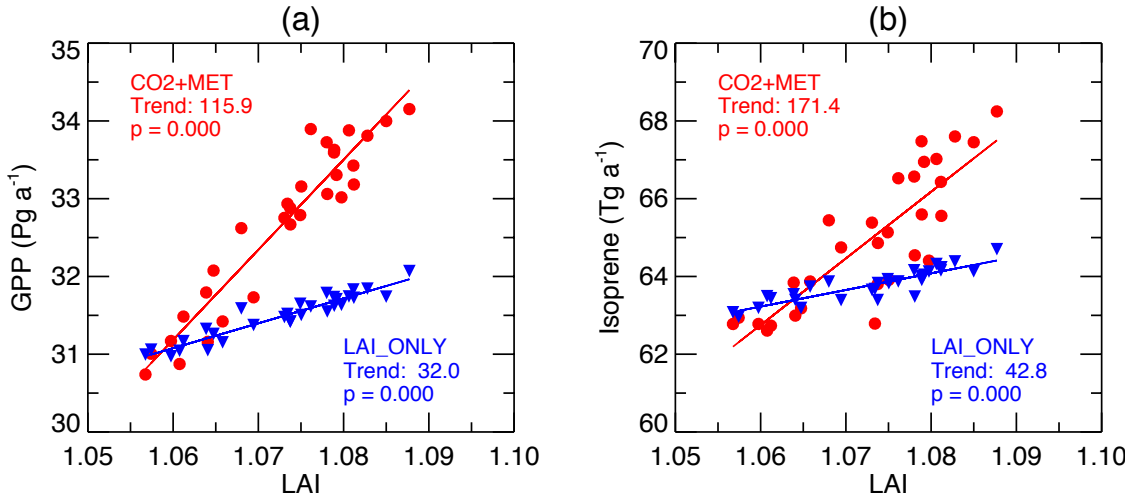

Figure 7. Responses of (a) GPP and (b) isoprene emissions to the changes in the annual average LAI at the north of 30°N for simulations CO2_MET (red) and LAI_ONLY (blue). Both GPP and isoprene emissions are the sum of all PFTs. Isoprene is simulated with the PS_BVOC scheme. Units of trends are (a) Pg C a^{-1} LAI^{-1} and (b) Tg C a^{-1} LAI^{-1}. The spatial distribution of GPP and isoprene changes is shown in Figure S2.

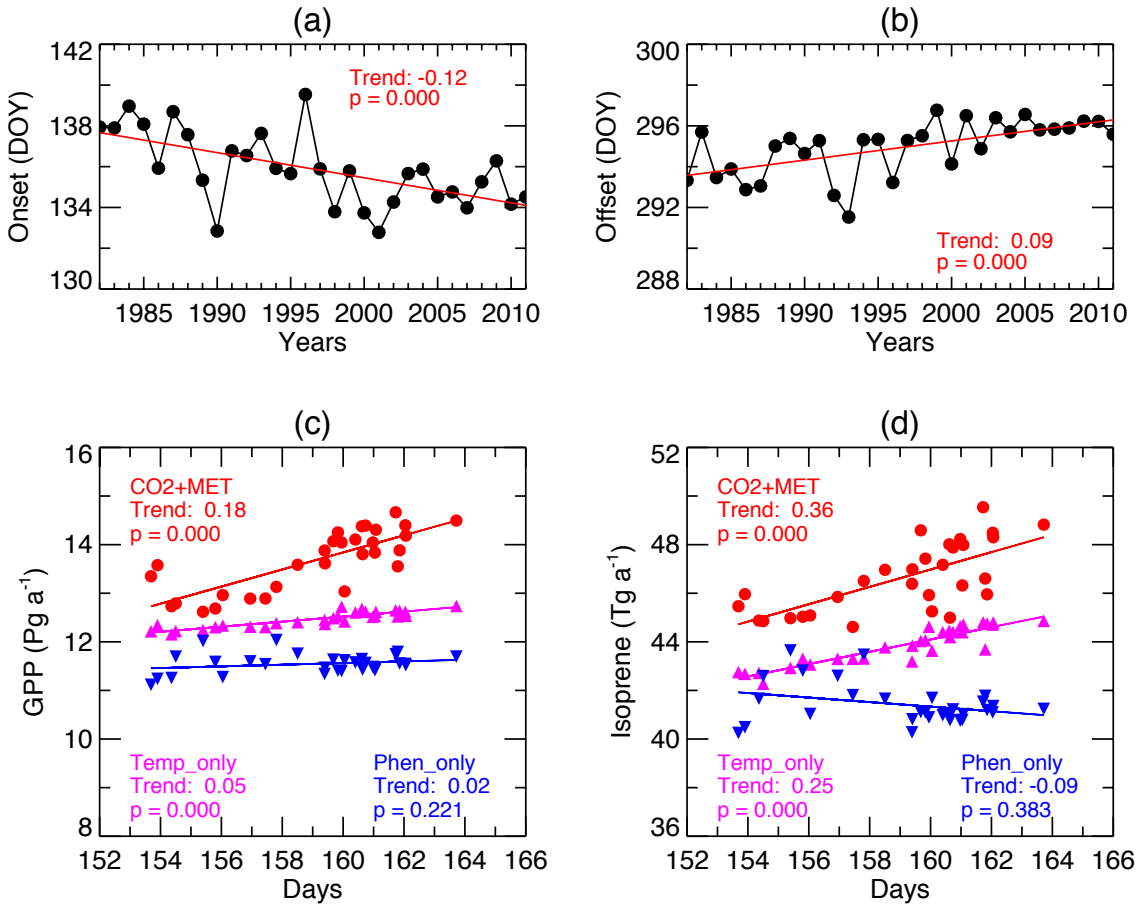

Figure 8. Predicted trend in (a) budburst and (b) dormancy onset dates over north of 30°N and the responses of (c) GPP and (d) isoprene emissions to the changes in the growing length. Both GPP and isoprene emissions are the sum of DBF, shrub, grassland, and tundra. Isoprene is simulated with the PS_BVOC scheme. For the bottom panel, different colors indicate sensitivity experiments with different year-to-year forcings: CO_2 and meteorology (red), temperature only (magenta), and phenology only (blue). Units of trends are (a) day a^{-1}, (b) day a^{-1}, (c) Pg C a^{-1} day^{-1}, and (d) Tg C a^{-1} day^{-1}. The spatial distribution of GPP and isoprene changes is shown in Figure S2.